

A&A manuscript no.

(will be inserted by hand later)

Your thesaurus codes are:

Interstellar Matter (02.18.7, 09.13.2., 09.19.1, 10.03.1, 11.14.1, 13.19.3)

ASTRONOMY  
AND  
ASTROPHYSICS  
2.1.2018

# Molecular Gas in the Galactic Center Region

## II. Gas mass and $\mathcal{N}_{\text{H}_2}/I_{12\text{CO}}$ conversion based on a $\text{C}^{18}\text{O}(J = 1 \rightarrow 0)$ Survey

G. Dahmen<sup>1,3</sup>, S. Hüttemeister<sup>2,4,1</sup>, T.L. Wilson<sup>1,5</sup>, R. Mauersberger<sup>6,1</sup>

<sup>1</sup> Max-Planck-Institut für Radioastronomie, Auf dem Hügel 69, 53121 Bonn, Germany

<sup>2</sup> Harvard-Smithsonian Center for Astrophysics, 60 Garden Street, Cambridge, MA 02138, U.S.A.

<sup>3</sup> Physics Department, Queen Mary & Westfield College, University of London, Mile End Road, London E1 4NS, England

<sup>4</sup> Radioastronomisches Institut, Universität Bonn, Auf dem Hügel 71, 53121 Bonn, Germany

<sup>5</sup> Submillimeter Telescope Observatory, The University of Arizona, Tucson, AZ 85721, U.S.A.

<sup>6</sup> Steward Observatory, The University of Arizona, Tucson, AZ 85721, U.S.A.

Received / Accepted

**Abstract.** The large scale structure and physics of molecular gas in the Galactic center region is discussed based on the detailed analysis of a  $9'$  resolution survey of the Galactic center region in the  $J = 1 \rightarrow 0$  line of  $\text{C}^{18}\text{O}$ . Emphasis is placed on the comparison with  $^{12}\text{CO}(1-0)$  data. The line shapes of  $\text{C}^{18}\text{O}(1-0)$  and  $^{12}\text{CO}(1-0)$  differ significantly. The ratio of the intensities of the two isotopomers in the Galactic center region is generally higher than the value of  $\sim 15$  expected from the “Standard Conversion Factor” (SCF) of  $^{12}\text{CO}$  integrated line intensity to  $\text{H}_2$  column density. In the  $9'$ -beam, this ratio is in the range from 30 to 200, mostly  $\sim 60$  to 80. From LVG calculations, we estimate that the large scale  $^{12}\text{CO}(1-0)$  emission in the Galactic center region is of moderate ( $\tau \gtrsim 1$ ) or low optical depth ( $\tau < 1$ ). Higher optical depths ( $\tau \geq 10$ ) are restricted to very limited regions such as Sgr B2. In addition, we estimate  $\text{H}_2$  densities and kinetic temperatures for different ranges of intensity ratios. A considerable amount of molecular mass is in a widespread molecular gas component with low densities and high kinetic temperatures. From our  $\text{C}^{18}\text{O}$  measurements and from results based on dust measurements, the total molecular mass is found to be  $(3_{-1}^{+2}) \cdot 10^7 M_{\odot}$ . We show that the SCF is *not* valid toward the Galactic bulge. It overestimates the  $\text{H}_2$  column density by an order of magnitude because the assumptions required for this factor of optically thick  $^{12}\text{CO}$  emission and virialization of the molecular clouds are not fulfilled for a significant fraction of the molecular gas. Therefore, also one cannot apply a modified conversion factor to the Galactic center region since the  $\mathcal{N}_{\text{H}_2}/I_{12\text{CO}}$  is highly variable and cannot be represented by a univer-

sal constant. Results from external galaxies indicate that the  $^{12}\text{CO}$  emission is generally not a suitable tracer of  $\text{H}_2$  masses in galactic bulges.

---

**Key words:** Radiative transfer — ISM: molecules, structure — Galaxy: center — Galaxies: nuclei — Radio lines: ISM

### 1. Introduction

Molecular clouds close to the center of our Galaxy are distinctly different from molecular material in the disk. Being dense, hot and highly turbulent (see, e.g., Hüttemeister et al. 1993), they constitute a third type of molecular environment besides cold and dense dark clouds and the warm and less dense surroundings of H II regions found in the Galactic disk. Within an area of a few hundred parsecs, these clouds concentrate  $\sim 10\%$  of the total neutral gas mass of the Galaxy (see, e.g., Güsten 1989). However, the properties of the molecular gas in this central region are less understood than other regions of the Milky Way.

Particularly important is the determination of the mass of molecular clouds, 70% of which is made up by molecular hydrogen,  $\text{H}_2$ . However,  $\text{H}_2$  lacks a permanent dipole moment and, hence, allowed rotational dipole transitions. Thus, the presence and properties of  $\text{H}_2$  in molecular clouds must be deduced from “tracer molecules” with permanent dipole moments. Such analyses must account for the excitation effects and the abundance of the molecules which produce the observable lines.

The most abundant molecule in the ISM with permanent dipole moment is carbon monoxide (see, e.g., Irvine

---

Send offprint requests to: S. Hüttemeister, Radioastronomisches Institut, Universität Bonn

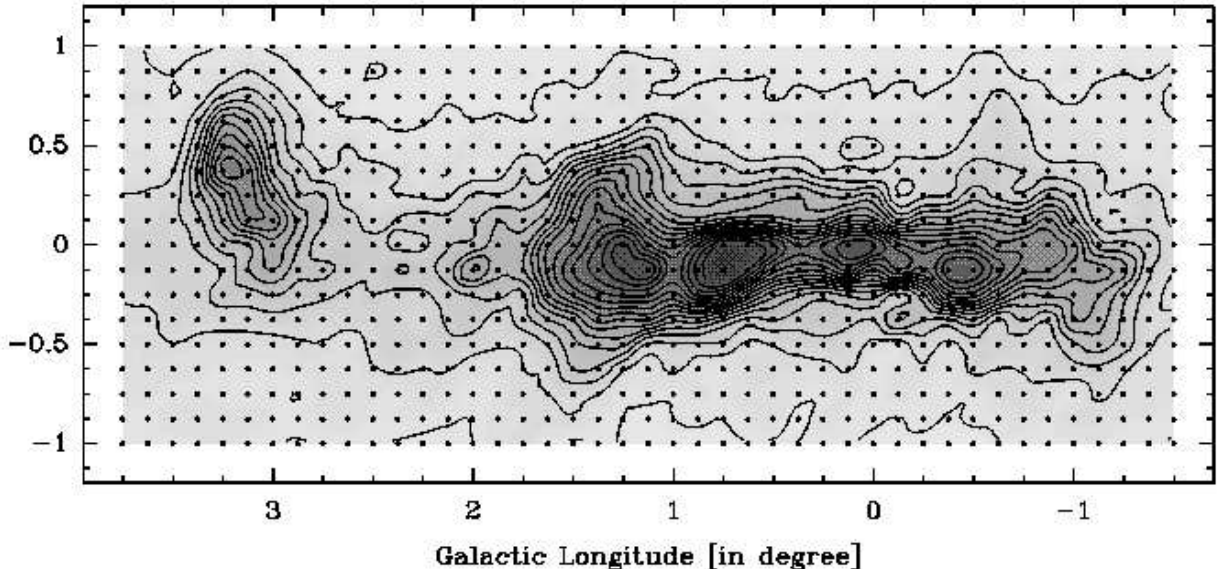


**Fig. 1.** The integrated intensity of the Galactic center region in  $\text{C}^{18}\text{O}(1-0)$  (from Paper I). The velocity over which the intensity (in  $T_{\text{MB}}$ ) is integrated ranges from  $-225.0$  to  $+225.0$   $\text{km s}^{-1}$ . The solid contour levels range from  $3.9$  to  $28.05$  in steps of  $3.45$   $\text{K km s}^{-1}$  where the lowest level is the  $3\sigma$ -value. The dashed contour is at  $2.6$   $\text{K km s}^{-1}$  which is the  $2\sigma$ -value. The circle in the lower left corner of the plot indicates the beam size of  $9'2$ .

et al. 1985). Because of the low critical density,  $n^*$ , of its  $J = 1 \rightarrow 0$  line of about  $740 \text{ cm}^{-3}$ , CO traces even the low-density molecular phase of the ISM. However, the emission of the main isotopomer  $^{12}\text{C}^{16}\text{O}$  is in most cases optically thick making it difficult to determine the volume and column densities from its emission lines. A comparison of  $^{12}\text{CO}^1$  with  $^{13}\text{CO}$  maps from large scale surveys in the  $J = 1 \rightarrow 0$  line in our Galaxy and external galaxies has shown that the line shapes and intensity ratios along different lines of sight are remarkably similar for both isotopomers, and the ratio of the CO isotopomer intensities varies remarkably little for different regions in the Galaxy (Dickman 1975; Young & Scoville 1982; Sanders et al. 1984). Because the weaker  $^{13}\text{CO}(1-0)$  line was usually assumed to be optically thin and, therefore, to trace the column density of  $\text{H}_2$  directly, it was concluded that the  $^{12}\text{CO}$  luminosity,  $L_{12\text{CO}(1-0)}$ , also measures mass, even though this line is optically thick (see, e.g., Dame 1993). This empirical  $^{12}\text{CO}$ -mass relation was confirmed, among other things, by comparison with  $\gamma$ -ray fluxes emitted when cosmic rays interact with  $\text{H}_2$  molecules (Bloemen et al. 1986) and by comparison with virial masses of Galactic and extragalactic clouds determined from their diameters and velocity dispersion (Solomon et al. 1987).

At first glance, it seems paradoxical that an optically thick transition can give information about the total column density of  $\text{H}_2$ . The paradox can be solved if one as-

sumes that there are several clouds within a beam area, the emission of which does not overlap in space and velocity (i.e. “CO counts clouds”). Also, if virialized, more massive clouds have more turbulence and, hence, a larger linewidth. Finally, the denser the gas the higher is the excitation of the gas. All these effects combined can approximately explain the observed relation (see, e.g., Dickman et al. 1986; Taylor et al. 1993). A number of investigations have been used to calibrate  $L_{12\text{CO}(1-0)}$  to the total molecular mass, both for the disk of the Milky Way and for external galaxies. This has led to establishing the “Standard Conversion Factor” (hereafter SCF), a.k.a. X, by Strong et al. (1988) which relates the integrated intensity of  $^{12}\text{CO}(1-0)$  to the  $\text{H}_2$  column density:

$$\bar{\mathcal{N}}_{\text{H}_2} = 2.3 \cdot 10^{20} \frac{\text{cm}^{-2}}{\text{K km s}^{-1}} \int T_{\text{MB}}^{12\text{CO}(1-0)} dv \quad (1)$$

We presented a large scale survey of the Galactic center region in the  $J = 1 \rightarrow 0$  line of  $\text{C}^{18}\text{O}$  obtained with the 1.2 m Southern Millimeter-Wave Telescope (SMWT) at the Cerro Tololo Interamerican Observatory (CTIO) near La Serena, Chile, in Dahmen et al. (1997), hereafter Paper I. Here, we carry out a more detailed analysis emphasizing the comparison to  $^{12}\text{CO}(1-0)$  data obtained with the same telescope. A summary of the conclusions was given in Dahmen et al. (1996). In Section 2, spectral line shapes toward selected positions are analyzed and ratios of integrated intensities of  $^{12}\text{CO}/\text{C}^{18}\text{O}$  are determined. In addition, we estimate optical depths, volume densities, and kinetic temperatures from Large Velocity Gradient (LVG) radiative transfer calculations. From these results,

<sup>1</sup> Following typical astronomical conventions, the atomic weight of the main isotopes will not be given explicitly, e.g.,  $^{13}\text{CO}$  and  $\text{C}^{18}\text{O}$ . However, for clarity we denote CO as  $^{12}\text{CO}$ .

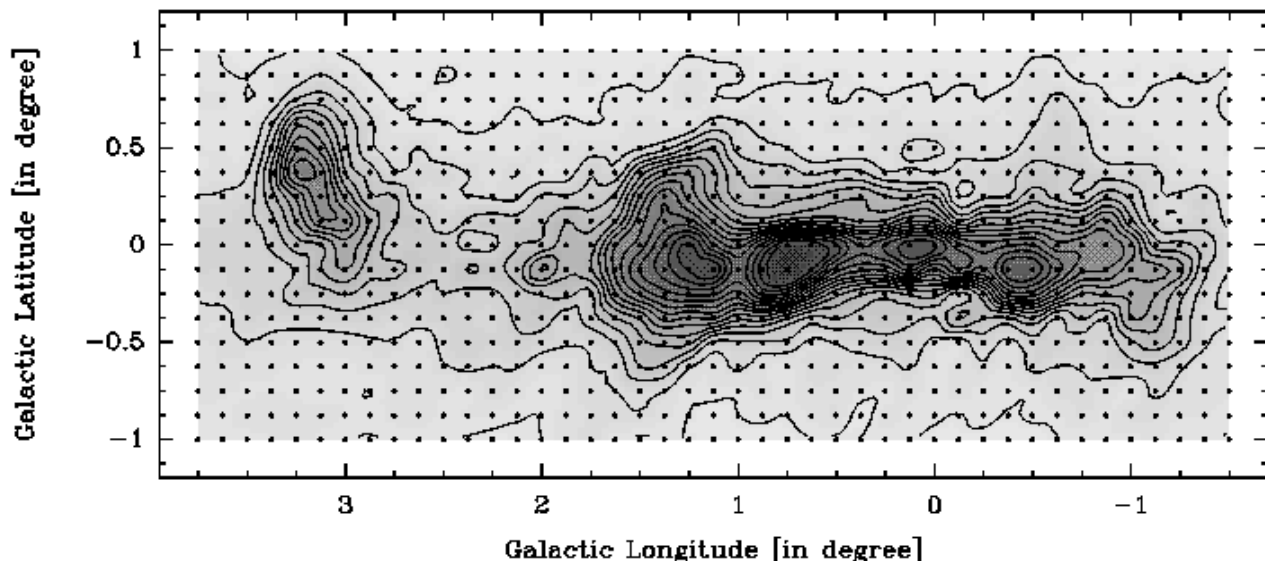


**Fig. 2.** The integrated intensity of the Galactic center region in  $^{12}\text{CO}(1-0)$  (data taken from Bitran 1987). The velocity the intensity (in  $T_{\text{MB}}$ ) is integrated over ranges from  $-225.0$  to  $+225.0$   $\text{km s}^{-1}$ . The plotted section ranges from  $l = -1.5$  to  $+3.75$  and from  $b = -1.0$  to  $+1.0$ . The solid contour levels range from  $50.0$  to  $1750.0$  in steps of  $100.0$   $\text{K km s}^{-1}$ . The minimum in the contour map is well above the  $3\sigma$ -value of about  $9.6$   $\text{K km s}^{-1}$ . The circle in the lower left corner of the plot indicates the beam size of  $8.8$ .

the  $\text{H}_2$  mass of the Galactic bulge is estimated. In Section 3, we compare our molecular mass to results based on dust measurements and give a *weighted best estimate* for the total molecular mass in the Galactic bulge. The consequences, e.g. for other galactic nuclei, are discussed. Finally, in Section 4, we present the conclusions drawn from our analysis.

Throughout this paper we adopt a distance to the Galactic center of  $8.5$  kpc.

## 2. Data and Analysis

The data of the  $\text{C}^{18}\text{O}(1-0)$  Galactic Center Survey were taken from August 1993 to August 1994 with the  $1.2$  m SMWT at CTIO. The survey covers the region  $-1.05 \leq l \leq +3.6$  and  $-0.9 \leq b \leq +0.75$  and has a spacing of  $9'$  which is the FWHP beamwidth (half sampling). A detailed description of these data and the observations is given in Paper I. In Fig. 1, we show the distribution of the integrated intensity of  $\text{C}^{18}\text{O}(1-0)$ , based on this survey.

For comparison, we used the  $^{12}\text{CO}(1-0)$  Galactic Center Survey, observed with the same telescope from February to November 1984 (Bitran 1987; Bitran et al. 1997). This survey covers a larger area than the region observed in  $\text{C}^{18}\text{O}$  and has a sampling of  $7.5$ . These data were made available to us in digital form, allowing a detailed analysis. A comparison of  $^{12}\text{CO}(1-0)$  data taken recently with the  $1.2$  m SMWT (see Paper I) with Bitran's observations

shows that the data sets are compatible (see Dahmen 1995 for the full account). The scaling factor to obtain  $T_{\text{MB}}$  from Bitran's  $T_{\text{A}}^*$  scale is  $1.11$  (see Dahmen 1995 for a discussion). In Fig. 2, we show the distribution of the integrated intensity of  $^{12}\text{CO}(1-0)$ , based on Bitran's data.

As shown in Paper I, the spectra and maps of the  $\text{C}^{18}\text{O}(1-0)$  survey demonstrate the great differences in the distribution of the optically thin  $\text{C}^{18}\text{O}(1-0)$  emission and the  $^{12}\text{CO}(1-0)$  emission, which is generally assumed to be optically thick. In addition, the  $^{12}\text{CO}$  emission is much more widespread than the  $\text{C}^{18}\text{O}$  emission whereas the  $\text{C}^{18}\text{O}$  emission shows much more contrast.

### 2.1. Spectral Line Shapes toward Selected Positions

In Fig. 3, we show spectra of both CO isotopomers toward characteristic emission centers, four examples of single positions toward the Galactic bulge and two of Clump 2 (Bania 1977) averaged over several positions to improve the signal-to-noise ratio of the weak  $\text{C}^{18}\text{O}$  emission. The  $^{12}\text{CO}$  spectra used were observed in March 1994 and August 1994 with the same SMWT setup as the  $\text{C}^{18}\text{O}$  Galactic Center Survey, as presented in Paper I. Throughout the Galaxy, the line shapes and intensity ratios of the optically thick  $^{12}\text{CO}$  and the optically thin  $^{13}\text{CO}$  transition along different lines of sight in the Galactic disk are remarkably similar, as mentioned in Section 1. This is also what should be the case if the SCF (Eq. 1) applies. However, in Appendix A.1 where we discuss the presented spectra in

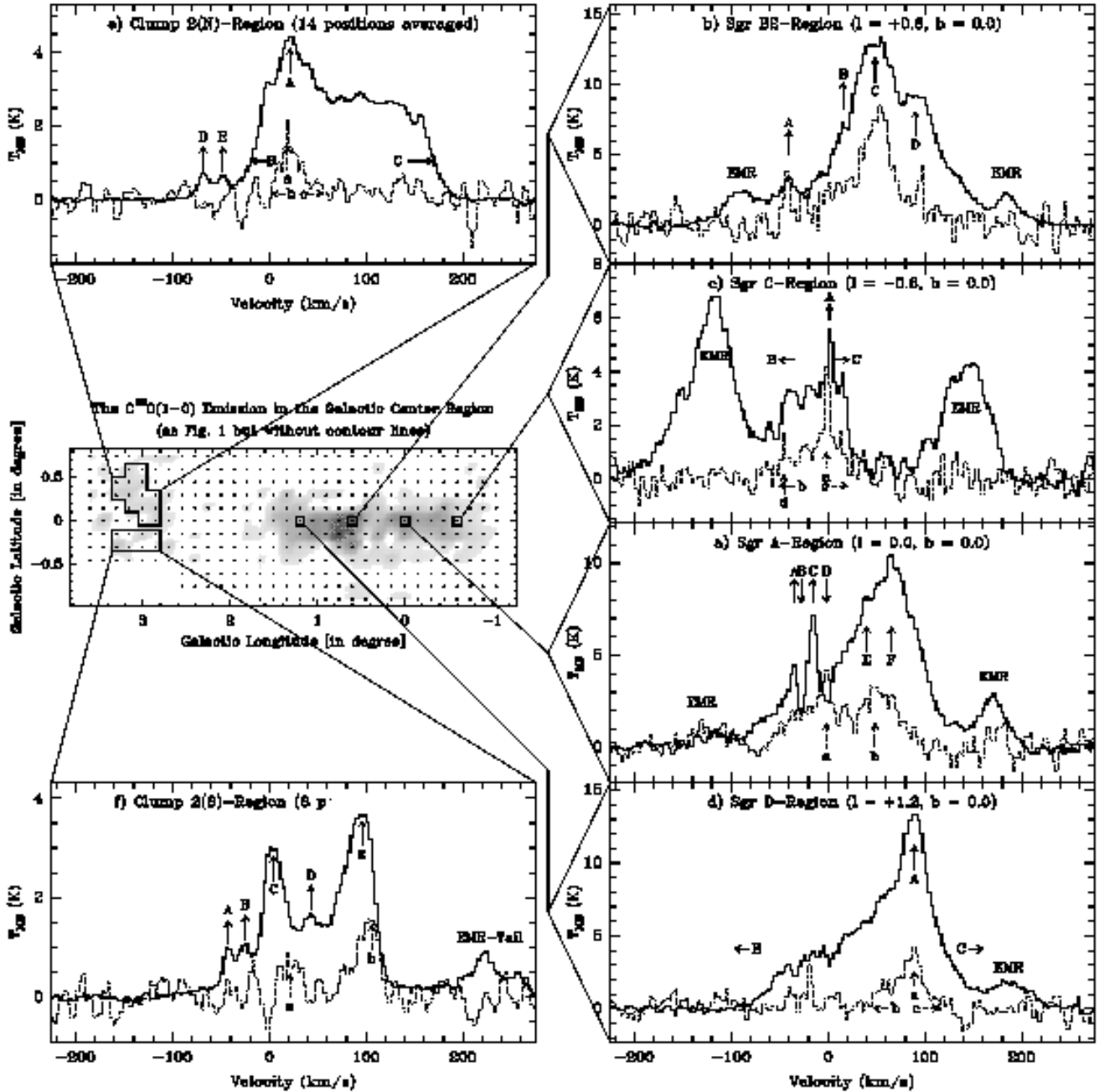


**Fig. 3.** CO isotopomer spectra toward characteristic emission centers. In all plots, the solid histogram is the spectrum of the  $^{12}\text{CO}(1-0)$  transition, while the dashed histogram is the spectrum of the  $^{13}\text{CO}(1-0)$  transition, multiplied by 20 for better comparability. Both were observed with the same SMWT setup during the  $^{13}\text{CO}$  Galactic Center Survey. Capital letters always mark features in  $^{12}\text{CO}$ , lower case letters features in  $^{13}\text{CO}$ . Upward pointing arrows indicate emission features, downward pointing arrows dips in the spectra. **a)** Position ( $l = 0^\circ.0$ ,  $b = 0^\circ.0$ ) near Sgr A. **b)** Position ( $l = +0^\circ.6$ ,  $b = 0^\circ.0$ ) near Sgr B2. **c)** Position ( $l = -0^\circ.6$ ,  $b = 0^\circ.0$ ) near Sgr C. **d)** Position ( $l = +1^\circ.2$ ,  $b = 0^\circ.0$ ) near Sgr D ( $l = 1^\circ.5$ -complex of Bally et al. 1988). **e)** Northern Clump 2 region (14 positions averaged as indicated). **f)** Southern Clump 2 region (8 positions averaged as indicated).

detail, we show that this is in many cases (e.g. plots (a), (c), (e) and (f) of Fig. 3) not true for the Galactic center  $^{12}\text{CO}$  and  $^{13}\text{CO}$ . Therefore, one or more of the requirements of this factor are not fulfilled (see also Section 3.2). This alone is proof that the  $J = 1 \rightarrow 0$  lines of  $^{12}\text{CO}$  and

$^{13}\text{CO}$  cannot both trace the total  $\text{H}_2$  mass in the Galactic center region, as it is commonly assumed for disk clouds. We also show that even toward positions where, at first, it appears that the SCF might be valid (e.g. plots (b) and (d) of Fig. 3) this is not the case. On the contrary, based on

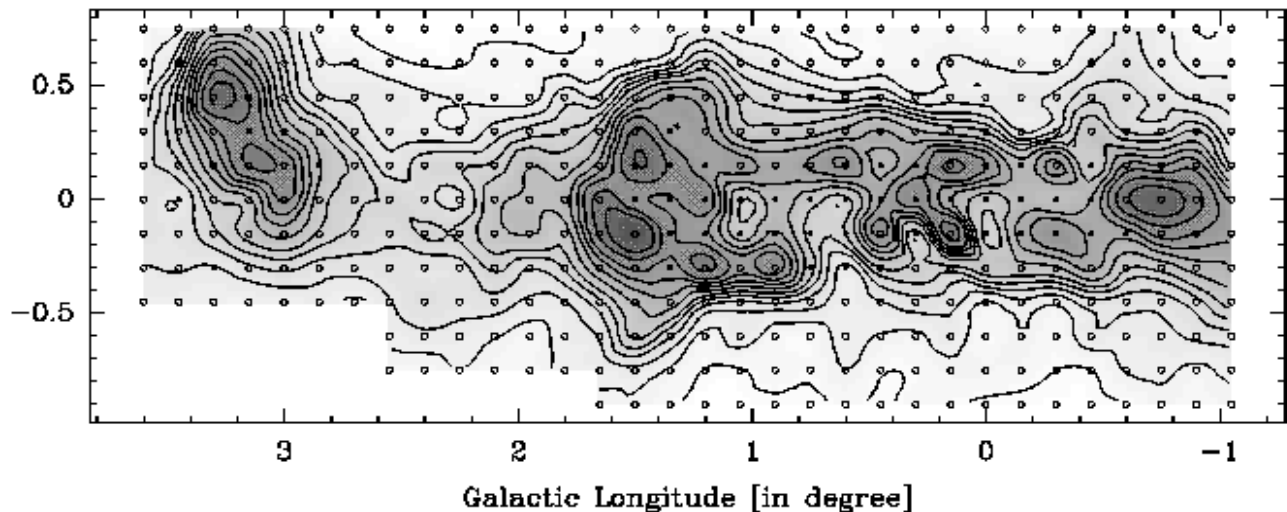


**Fig. 4.** The integrated intensity ratio of  $^{12}\text{CO}(1-0)$  to  $\text{C}^{18}\text{O}(1-0)$  emission in the Galactic center region. The intensities are integrated over a velocity range from  $-225.0$  to  $+225.0$   $\text{km s}^{-1}$ . The solid contour levels range from 10.0 to 60.0 in steps of 10.0, from 60.0 to 120.0 in steps of 15.0, and from 120.0 to 180.0 in steps of 20.0. The circle in the lower left corner of the plot indicates the averaged beam size of  $9'$ . The ratio was calculated with an  $3\sigma$ -threshold, thus, if the integrated intensity of  $\text{C}^{18}\text{O}$  was below  $3\sigma$  r.m.s. the  $3\sigma$  value was taken instead for the calculation of the ratio. Filled points indicate positions where  $\text{C}^{18}\text{O}$  is above this threshold. Open points indicate positions where  $\text{C}^{18}\text{O}$  is below this threshold, thus, positions where the calculated ratio is a lower limit.

an LTE analysis we show that the data suggest moderate optical depths ( $\tau \gtrsim 1$ ) for most of the  $^{12}\text{CO}$  emission, even toward very intense peaks, rather than very high optical depths ( $\tau \gg 1$ ) which is one of the essential requirements that the SCF is applicable. From these results, we conclude that in the Galactic center region:

- (1) the SCF for the determination of the  $\text{H}_2$  column density is not applicable;
- (2) the assumption of large optical depth for the  $^{12}\text{CO}(1-0)$  emission is not valid.

## 2.2. CO Integrated Intensity Ratios

From a comparison of Figs. 1 and 2, it is obvious that there are great differences in the spatial distribution of the integrated intensities of  $\text{C}^{18}\text{O}(1-0)$  and  $^{12}\text{CO}(1-0)$ . These differences become even larger if one compares the channel maps of integrated intensities (see Figs. 5 and 15 in Paper I) or the  $lv$ -plots (see Figs. 6 and 16 in Paper I). The  $\text{C}^{18}\text{O}$  emission has a distinctly larger contrast compared to the rather smooth  $^{12}\text{CO}$  emission. In this section, we investigate the variation in the intensity ratio of  $^{12}\text{CO}/\text{C}^{18}\text{O}$ , first integrated over the total velocity extent of CO emission, and then over velocity intervals of  $50$   $\text{km s}^{-1}$  width.

For this purpose, the  $^{12}\text{CO}(1-0)$  data of Bitran (1987) were resampled to the slightly lower velocity and spatial resolution of the  $\text{C}^{18}\text{O}$  spectra. Then, the integrated intensity ratios were determined by calculating the integrated intensities of  $^{12}\text{CO}$  and  $\text{C}^{18}\text{O}$  for the chosen velocity interval respectively and dividing the result for  $^{12}\text{CO}$  by the

result for  $\text{C}^{18}\text{O}$ . The ratios of the integrated intensities were calculated with a threshold set to 3 times the r.m.s. noise (see below for its value). Thus, if the integrated intensity in  $^{12}\text{CO}$  or in  $\text{C}^{18}\text{O}$  was below this  $3\sigma$ -limit, the  $3\sigma$ -value was taken instead. Because the  $^{12}\text{CO}$  emission is much more intense than the  $\text{C}^{18}\text{O}$  emission, there are areas where  $^{12}\text{CO}$  is present but  $\text{C}^{18}\text{O}$  is below the detection limit. In these cases, the determined ratio of the integrated intensities is a *lower limit* instead of the true value. Similarly, calculated ratios of the integrated intensities are *never* upper limits, hence, the true ratio is *never* lower than calculated (within the noise scatter). The lowest possible value is about 2.5, the ratio of the  $3\sigma$ -values (which is equivalent to no information on the ratio).

For  $^{12}\text{CO}$ , we used as the  $3\sigma$ -threshold the value which should statistically be achieved after integrating over the desired velocity range (and which is  $3 \cdot \sqrt{N_{ch}} v_{ch}$  r.m.s.ch; see also Eq. 2 in Paper I). This was  $14.2$   $\text{K km s}^{-1}$  in case of intensities integrated over of the total velocity range and  $4.9$   $\text{K km s}^{-1}$  in case of intensities integrated over velocity intervals of  $50$   $\text{km s}^{-1}$  width.

In case of  $\text{C}^{18}\text{O}$ , however, it turned out that this straight-forward method is not applicable. Because of systematic effects the noise in our data improves more slowly than the square root of the integration time. Thus, the true r.m.s. of the integrated intensities cannot be found as easily as in case of  $^{12}\text{CO}$ . It is, however, essential for our analysis that we do not use a threshold which is too low because in this case we might overestimate the  $^{12}\text{CO}/\text{C}^{18}\text{O}$  ratio instead of using a valid lower limit. Because our conclusions rely critically on high  $^{12}\text{CO}/\text{C}^{18}\text{O}$  ratios, we must

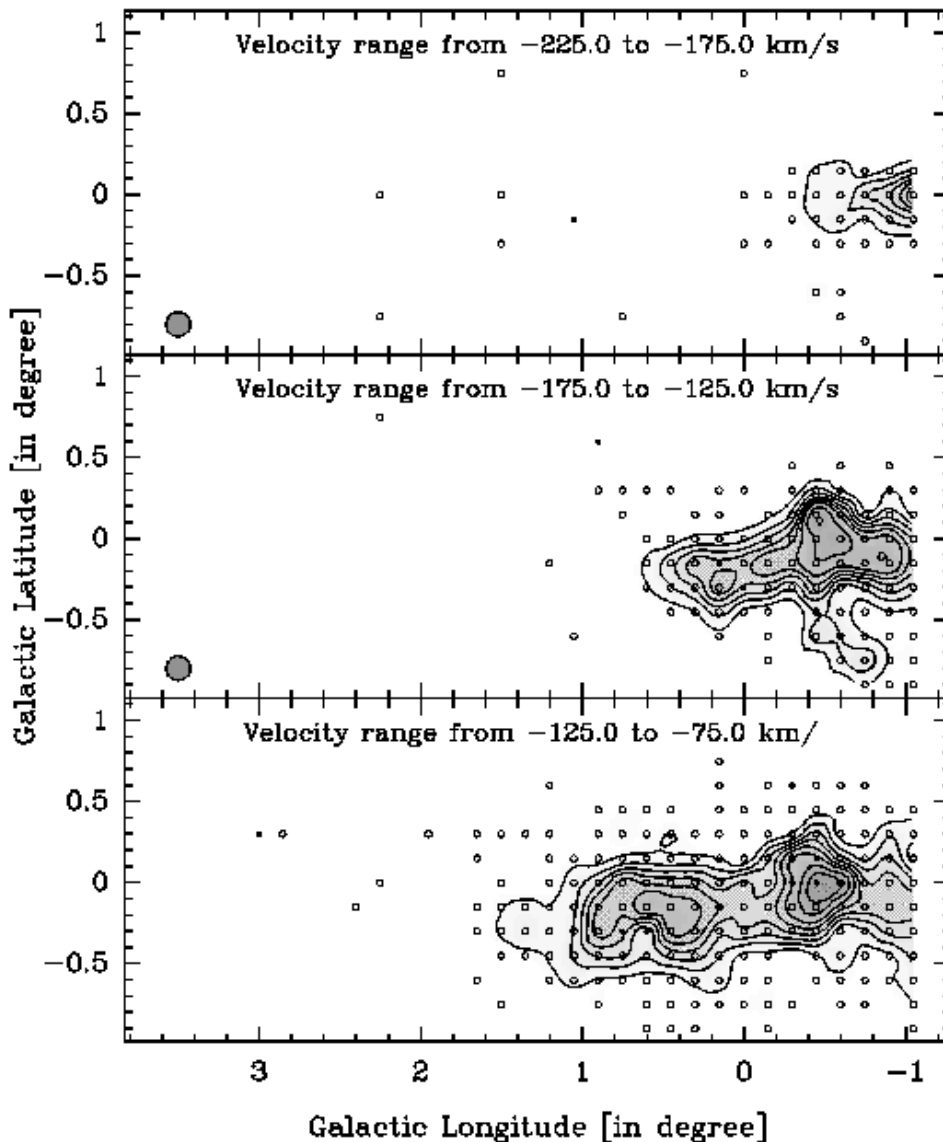


**Fig. 5.** The intensity ratio of  $^{12}\text{CO}(1-0)$  to  $\text{C}^{18}\text{O}(1-0)$  emission in the Galactic center region integrated over velocity intervals of  $50 \text{ km s}^{-1}$  width. The solid contour levels range from 10.0 to 60.0 in steps of 10.0, from 60.0 to 120.0 in steps of 15.0, and from 120.0 to 200.0 in steps of 20.0. The circle in the lower left corner of the plots indicates the averaged beam size of  $9'$ . The ratio was calculated with an  $3\sigma$ -threshold, thus, if the integrated intensity of either  $\text{C}^{18}\text{O}$  or  $^{12}\text{CO}$  was below  $3\sigma$  r.m.s. the  $3\sigma$  value was taken instead for the calculation of the ratio. Filled points indicate positions where both  $\text{C}^{18}\text{O}$  and  $^{12}\text{CO}$  are above the threshold. Open points indicate positions where  $\text{C}^{18}\text{O}$  is below the threshold but where  $^{12}\text{CO}$  emission is seen, thus, where the calculated ratio is a lower limit. Where both  $\text{C}^{18}\text{O}$  and  $^{12}\text{CO}$  are below the threshold, no statement about the  $^{12}\text{CO}/\text{C}^{18}\text{O}$  ratio can be made, so these positions are not indicated. **a)** At the top the integrated intensity ratio of the velocity range from  $-225.0$  to  $-175.0 \text{ km s}^{-1}$  is plotted, in the middle panel the velocity ranges from  $-175.0$  to  $-125.0 \text{ km s}^{-1}$ , and at the bottom the velocity range from  $-125$  to  $-75.0 \text{ km s}^{-1}$  is shown.

be certain that we never overestimate this ratio. Therefore, we have to determine the r.m.s. of the integrated intensities empirically. We carried this out by calculating the r.m.s. deviation of the intensities integrated over velocity intervals of  $50 \text{ km s}^{-1}$  width for the positions from  $l = -1^{\circ}05$  to  $+2^{\circ}1$  at  $b = +0^{\circ}75$ . These 22 positions

are ensured to be emission-free in  $\text{C}^{18}\text{O}$  over the complete velocity interval. We find an r.m.s. of  $0.65 \text{ K km s}^{-1}$ . Hence, we choose as  $3\sigma$ -threshold for  $\text{C}^{18}\text{O}$  intensities integrated over velocity intervals of  $50 \text{ km s}^{-1}$  a value of  $2.0 \text{ K km s}^{-1}$ . Similarly, we find the  $3\sigma$ -threshold for  $\text{C}^{18}\text{O}$

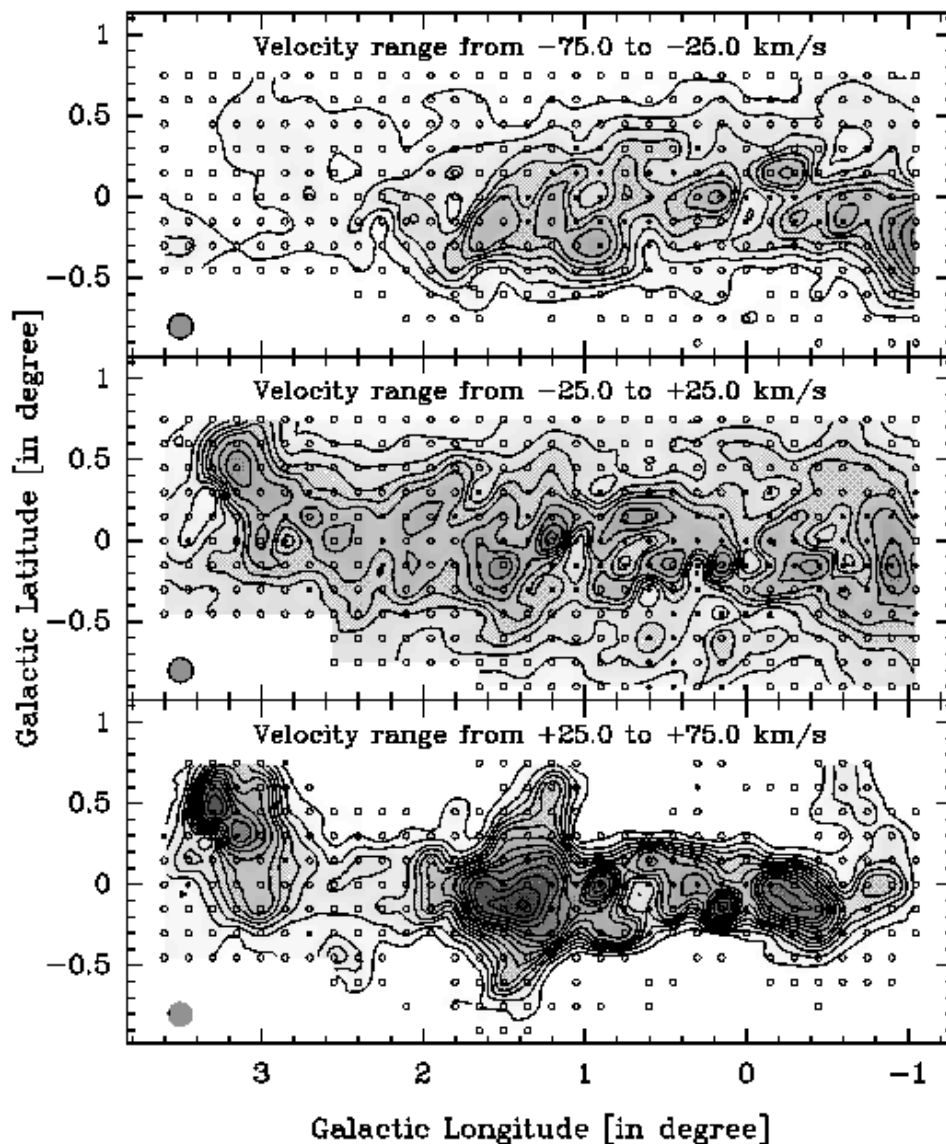


Fig. 5. b) At the top the integrated intensity ratio of the velocity range from  $-75.0$  to  $-25$   $\text{km s}^{-1}$  is plotted, in the middle panel the velocity ranges from  $-25$  to  $+25$   $\text{km s}^{-1}$ , and at the bottom the velocity range from  $+25$  to  $+75.0$   $\text{km s}^{-1}$  is shown.

intensities integrated over of the total velocity range to be  $5.9$   $\text{K km s}^{-1}$ .

In Fig. 4, we plot the ratio of the  $^{12}\text{CO}(1-0)$  to  $\text{C}^{18}\text{O}(1-0)$  intensity in the Galactic center region, integrated over the total velocity interval from  $-225.0$  to  $+225.0$   $\text{km s}^{-1}$ . The ratio of the integrated intensities shows a large variation from 30 to 190. The most prominent maxima are the Sgr D region ( $l = 1^\circ 5$ -complex of Bally et al. 1988) with ratios up to 190 at ( $l = +1^\circ 5$ ,  $b = -0^\circ 15$ ), the region somewhat west of Sgr C with ratios up to 175 at ( $l = -0^\circ 75$ ,  $b = 0^\circ 0$ ), and Clump 2 with ratios up to 165 at ( $l = +3^\circ 3$ ,  $b = +0^\circ 45$ ). On the other hand, true minima (not lower limits), valley-like

surrounded by higher ratios, are visible toward the regions of Sgr A and Sgr B2 and toward the region at ( $l = +1^\circ 05$ ,  $b = 0^\circ 0$ ).

High integrated intensity ratios tend to coincide with strong CO emission. Since high ratios are correlated with low optical depths in both  $^{12}\text{CO}(1-0)$  and  $\text{C}^{18}\text{O}(1-0)$  (Eq. A6), one might expect these maxima to be correlated with weak CO emission. However, at positions where the  $^{12}\text{CO}$  emission is weak, the strength of the  $\text{C}^{18}\text{O}$  emission might be *far below* the  $3\sigma$ -threshold, thus, the determined *lower limit* for the integrated intensity ratio might underestimate the true ratio *by far*.

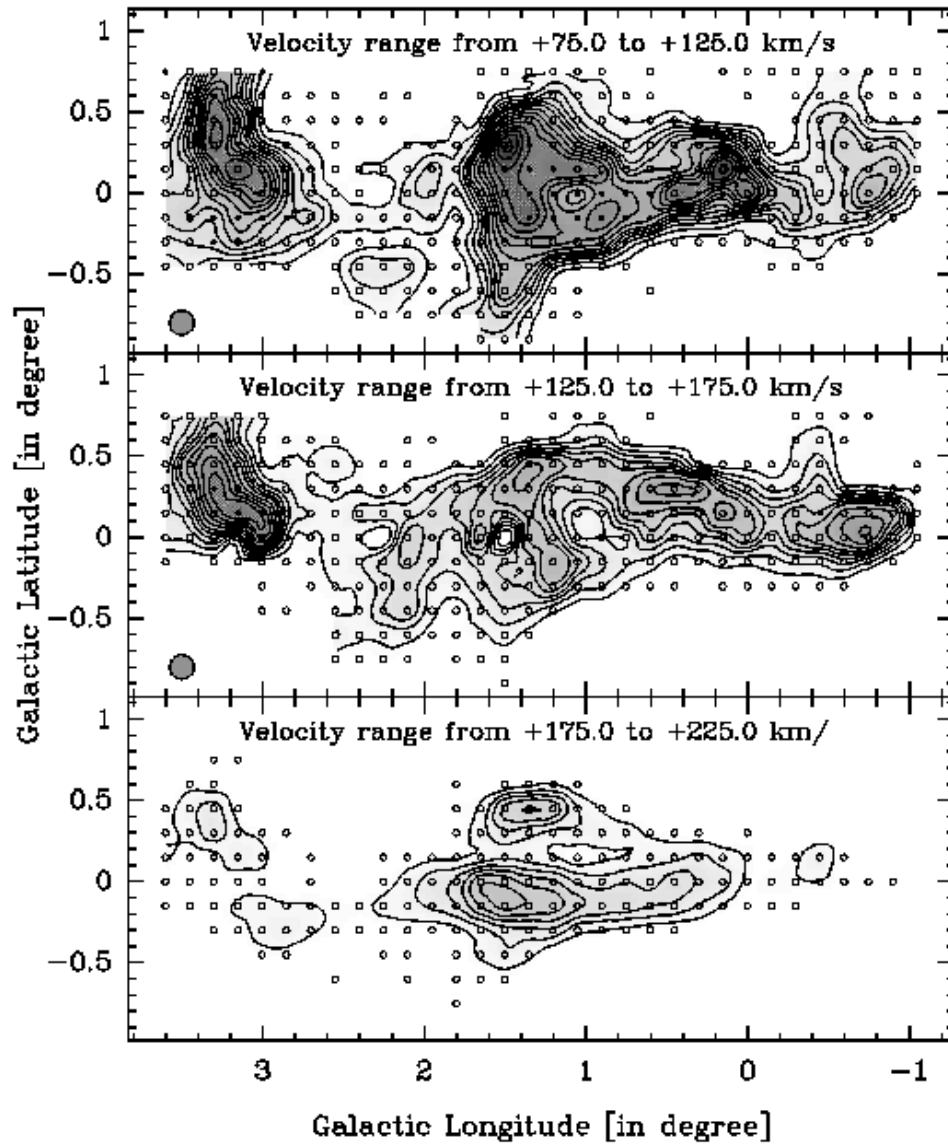


Fig. 5. c) At the top the integrated intensity ratio of the velocity range from +75.0 to +125  $\text{km s}^{-1}$  is plotted, in the middle panel the velocity ranges from +125 to +175  $\text{km s}^{-1}$ , and at the bottom the velocity range from +175 to +225.0  $\text{km s}^{-1}$  is shown.

In Fig. 5, we show the ratios of  $^{12}\text{CO}(1-0)$  to  $\text{C}^{18}\text{O}(1-0)$  intensities integrated over velocity intervals of  $50 \text{ km s}^{-1}$  width. While already the ratio of the intensities integrated over the total velocity interval shows a large variation and a lot of structure this is even more so in the  $50 \text{ km s}^{-1}$ -interval maps. In addition, the ratio in the channel maps reaches values up to  $> 200$ .

In Appendix A.2, we give a detailed description of the features visible. This analysis shows that the integrated intensity ratio of  $^{12}\text{CO}/\text{C}^{18}\text{O}$  in the Galactic center region is generally higher than the value of  $\sim 15$  expected from the “standard” conversion factors. Wherever  $\text{C}^{18}\text{O}$

is above the detection limit, this ratio is at least of order 40, mostly of order of 60 to 80, in several areas of order 90 to 120, and toward a few positions even up to  $> 200$ . Note that these values are an average over an area of  $9'$  diameter. Therefore, we conclude that high  $^{12}\text{CO}/\text{C}^{18}\text{O}$  ratios are typical of the molecular gas in the Galactic center region. Ratios as low as expected from the “standard” conversion factors are rare and restricted to rather small areas in the Galactic center. For example, from measurements with the IRAM 30 m telescope ( $23''$  resolution) Mauersberger et al. (1989) found a  $^{12}\text{CO}/\text{C}^{18}\text{O}$  ratio of 13 toward Sgr B2. Thus, if the beam is small and the observation



carried out toward the peak of an exceptional region, the ratio can be in agreement with the standard conversion. However, averaged over the 9'-beam of the 1.2 m SMWT, the ratio is  $\lesssim 40$  (see Appendix A.2). Thus, the lower ratio is found only in a very limited area close to the peak of Sgr B2.

### 2.3. LVG Calculations on the CO Isotopomer Ratio

In this section, we carry out radiative transfer calculations for the excitation of the  $J = 1 \rightarrow 0$  transition of  $^{12}\text{CO}$  and  $\text{C}^{18}\text{O}$  using the Large Velocity Gradient (LVG) approximation with collision rates taken from Green & Chapman (1978) to explore non-LTE conditions (see, e.g., de Jong et al. (1975) or Rohlfs & Wilson (1996), chapter 14.10, for a full description of radiative transfer in the LVG approximation). The LVG radiative transfer program used was kindly provided by C. Henkel; see Henkel (1980) for a full description of the program.

For optically thin  $\text{CO}(1-0)$ , the thermalization density is about  $740 \text{ cm}^{-3}$ ; the highest density for which CO intensities change significantly with  $\text{H}_2$  density is  $\sim 10^4 \text{ cm}^{-3}$ . The fits were always performed with the  $^{12}\text{CO}/\text{H}_2$  ratio assumed to be  $10^{-4}$  and the  $\text{C}^{18}\text{O}/\text{H}_2$  to be  $4 \cdot 10^{-7}$ , thus, the  $^{12}\text{CO}/\text{C}^{18}\text{O}$  was assumed to be 250, since this is the commonly accepted value for the Galactic center region (Wilson & Matteucci 1992; Wilson & Rood 1994). See the caption of Fig. 6 for more details.

Because this investigation is focused on the optical depth, the program was modified to fit an optical depth in the  $^{12}\text{CO}(1-0)$  transition to given input parameters by varying the velocity gradient and fixing all the other parameters ( $n_{\text{H}_2}$ ,  $T_{\text{kin}}$ ,  $X$ , and  $T_{\text{C}}$ ). The velocity gradient determined for the optical depths of the  $^{12}\text{CO}(1-0)$  transition was taken as an input parameter for the respective  $\text{C}^{18}\text{O}$  calculations. The calculated optical depths for the  $\text{C}^{18}\text{O}(1-0)$  transition were always  $\ll 1$ , confirming the notion that the  $\text{C}^{18}\text{O}(1-0)$  transition is always optically thin. The results of the LVG calculations are plotted in Fig. 6.

In Section 2.2, we distinguish four intensity ratio ranges: low ratios of about 40 (a few positions), intermediate ratios of 60 to 80 (widespread), high ratios of 90 to 120 (several areas), and very high ratios up to  $> 200$  (a few positions). From Fig. 6, one can see that high  $^{12}\text{CO}/\text{C}^{18}\text{O}$  intensity ratios are usually correlated with lower optical depth in the  $^{12}\text{CO}(1-0)$  transition. In addition, for higher kinetic temperatures high  $^{12}\text{CO}/\text{C}^{18}\text{O}$  intensity ratios are more restricted to low densities. However, these are only trends, and one can find an appropriate optical depth to fit the required intensity ratio for nearly every pair of  $\text{H}_2$  density and  $T_{\text{kin}}$ . Therefore, one needs an additional restriction on the possible range of  $\text{H}_2$  density and  $T_{\text{kin}}$ . This can be the velocity gradient which, from the fits, covers an unrealistically large range from  $0.004 \text{ km s}^{-1} \text{ pc}^{-1}$  to  $462 \text{ km s}^{-1} \text{ pc}^{-1}$ . A reasonable gradient can be estimated from the typical velocity extent and diameter of molec-

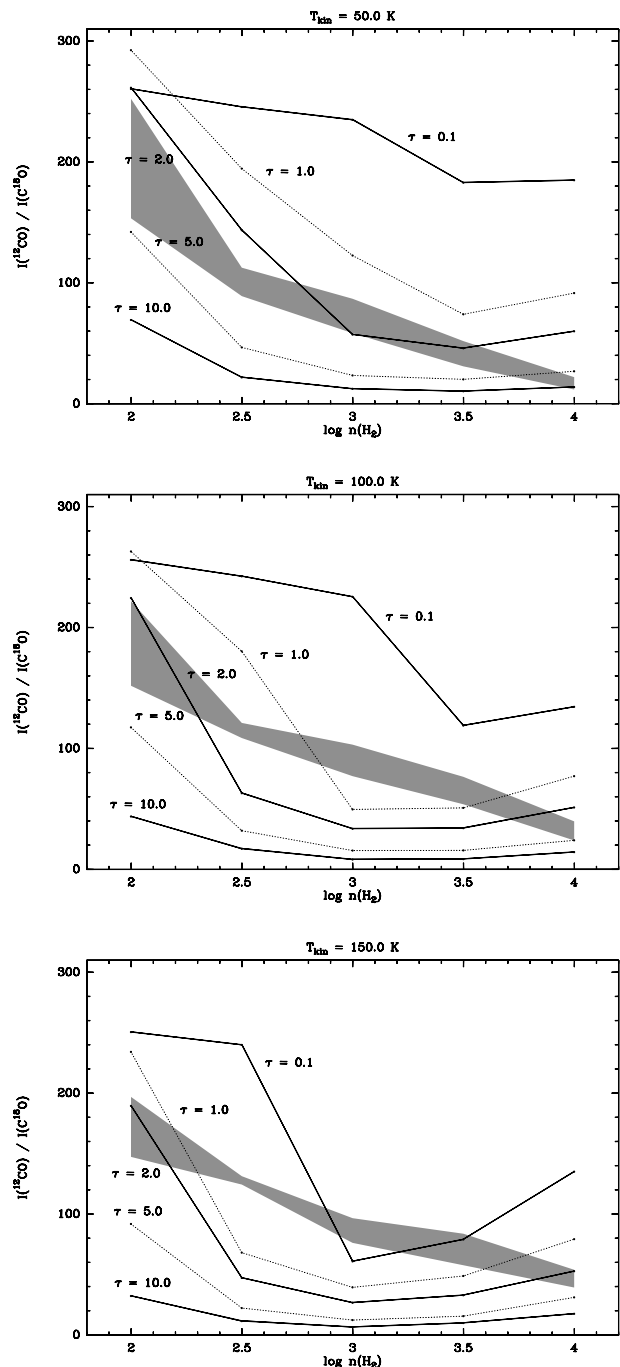


**Fig. 6.** The predicted  $^{12}\text{CO}/\text{C}^{18}\text{O}$  intensity ratios in the  $J = 1 \rightarrow 0$  transition as a function of the  $\text{H}_2$  density for  $T_{\text{kin}} = 50.0 \text{ K}$ ,  $100.0 \text{ K}$ , and  $150.0 \text{ K}$  from LVG calculations. The ratios are determined for optical depths of 0.1, 1.0, 2.0, 5.0, and 10.0 in the  $^{12}\text{CO}(1-0)$  transition, with  $[^{12}\text{CO}/\text{H}_2] = 10^{-4}$  and  $[^{12}\text{CO}/\text{C}^{18}\text{O}] = 250$ . The temperature of continuum background radiation,  $T_{\text{C}}$ , was chosen to be the cosmic background radiation of 2.7 K. The shaded area indicates the velocity gradient range from  $3 \text{ km s}^{-1} \text{ pc}^{-1}$  to  $6 \text{ km s}^{-1} \text{ pc}^{-1}$ , which is the most likely value for the Galactic center region.

ular clouds in the Galactic center as it is found in the higher resolution maps of  $^{13}\text{CO}(1-0)$  (Bally et al. 1987) and  $\text{C}^{18}\text{O}(1-0)$  (Lindqvist et al. 1995). With a typical velocity extent of  $30 \text{ km s}^{-1}$  to  $50 \text{ km s}^{-1}$  and a diameter of  $2'$  to  $5'$ , keeping in mind that larger cloud diameters are correlated to larger velocity extents, we estimate that the velocity gradient of Galactic center clouds typically ranges from  $3 \text{ km s}^{-1} \text{ pc}^{-1}$  to  $6 \text{ km s}^{-1} \text{ pc}^{-1}$ . This range is shown shaded in Fig. 6.

The range of  $\text{H}_2$  density and  $T_{\text{kin}}$  is now rather strongly limited and more definite parameters for the four ranges of intensity ratios can be estimated. For all three  $T_{\text{kin}}$  values, the allowed  $^{12}\text{CO}/\text{C}^{18}\text{O}$  intensity ratio declines monotonically with increasing  $\text{H}_2$  densities. To get estimates for  $\text{H}_2$  density and  $T_{\text{kin}}$  of the ratio ranges, we discuss each range separately taking into account additional information from other observations:

- (1) For low intensity ratios of about 40, a fairly high  $\text{H}_2$  density is predicted. For  $T_{\text{kin}} = 50 \text{ K}$ ,  $n_{\text{H}_2} > 10^{3.3} \text{ cm}^{-3}$  is required. For higher  $T_{\text{kin}}$ , this value is even larger. Hüttemeister et al. (1993) suggested the existence of two gas components: a cool ( $T_{\text{kin}} \approx 25 \text{ K}$ ) component with higher density and a hot ( $T_{\text{kin}} \approx 200 \text{ K}$ ) component with lower density. Because the positions studied by Hüttemeister et al. were centered on the CS(2-1) peak positions of Bally et al. (1987), they argued that CS in the cool and denser component should be thermalized, with  $\text{H}_2$  densities above  $1.8 \cdot 10^4 \text{ cm}^{-3}$ . Away from such peak positions, averaged over the  $9'$ -beam, densities should be lower, perhaps by a factor of 5 to 10. Similarly,  $T_{\text{kin}}$  should be slightly higher. Therefore, we favor a beam averaged  $\text{H}_2$  density of  $\sim 10^{3.5} \text{ cm}^{-3}$ , a kinetic temperature of  $\sim 50 \text{ K}$ , and a  $^{12}\text{CO}$  optical depth of  $\sim 3.0$  for those regions showing low intensity ratios.
- (2) Intermediate ratios of 60 to 80 are most common, especially at  $-50 \text{ km s}^{-1}$  and  $0 \text{ km s}^{-1}$ , and should, therefore, not have a density above the average. If the extent of the molecular emission along the line of sight is comparable to the longitudinal extent of the bulge region and if the scale height of the the molecular emission is  $\sim 0.2$ , the mean  $\text{H}_2$  density is (with a total gas mass of  $3 \cdot 10^7 M_{\odot}$ , determined in Section 3.1)  $\sim 150 \text{ cm}^{-3}$ . However, some clumping is expected. For  $T_{\text{kin}} = 50 \text{ K}$ , the LVG results require  $n_{\text{H}_2} > 10^{2.8} \text{ cm}^{-3}$ ; for higher  $T_{\text{kin}}$ , this value will be even larger. Therefore, we estimate that the most appropriate (and lowest possible) density for this intensity range is  $n_{\text{H}_2} \approx 10^{3.0} \text{ cm}^{-3}$ , at  $T_{\text{kin}} = 50 \text{ K}$  and  $\tau_{12\text{CO}} < 2.0$ .
- (3) For high ratios of 90 to 120, the LVG calculations require  $\text{H}_2$  densities of an order of magnitude lower than in case (1) for the same  $T_{\text{kin}}$  values. Since (following Hüttemeister et al. 1993) it is more likely that  $T_{\text{kin}}$  is larger for gas with lower density, but since the ratios considered here are not the highest, we estimate that  $T_{\text{kin}}$  is  $\sim 100 \text{ K}$ . This implies an  $\text{H}_2$  density of

$\sim 10^{3.0} \text{ cm}^{-3}$  and  $\tau_{12\text{CO}} < 1.0$ . For Clump 2, this result is confirmed by Stark & Bania (1986) who found an optical depth of less than unity from a comparison of  $^{12}\text{CO}(1-0)$  to  $^{13}\text{CO}(1-0)$  emission using the usually assumed isotope ratio of  $^{12}\text{C}/^{13}\text{C} = 20$  (Penzias 1980; Wilson & Matteucci 1992; Wilson & Rood 1994).

- (4) For very high ratios up to over 200, the LVG results require an  $\text{H}_2$  density of  $n_{\text{H}_2} < 10^{2.5} \text{ cm}^{-3}$ . We favor a  $T_{\text{kin}} \approx 150 \text{ K}$  for this low density gas as the beam-averaged value of the hot ( $T_{\text{kin}} \approx 200 \text{ K}$ ) low density component found by Hüttemeister et al. (1993). This implies an  $\text{H}_2$  density of  $\sim 10^{2.0} \text{ cm}^{-3}$  and an optical depth of  $\sim 2.0$ . Such a high value of  $T_{\text{kin}}$  is supported by calculations of Flower et al. (1995) who estimated  $T_{\text{kin}} \approx 500 \text{ K}$  for the low density envelope of Sgr B2. Hence, even in our  $9'$ -beam  $150 \text{ K}$  seems to be a reasonable value of  $T_{\text{kin}}$ .

We list our best estimates of the physical parameters in the four line intensities ratio ranges in Table 1. Note that the large beam *averages* over a wide range of environments. Thus, the derived values indicate which conditions dominate within the  $9'$ -beam. This does not mean that they are exclusively present as can be seen in a detailed analysis of high density peaks (Hüttemeister et al. 1997).

**Table 1.** Best estimates for beam averaged gas parameters for four ranges of line intensity ratios, based on LVG calculations

$I_{12\text{CO}}/I_{\text{C}^{18}\text{O}}$	$\log(n_{\text{H}_2})$ [ $\text{cm}^{-3}$ ]	$T_{\text{kin}}$ [K]	$\tau_{12\text{CO}}$
$\lesssim 40$	3.5	50	$\sim 3.0$
<b>60 – 80</b>	3.0	50	$< 2.0$
<b>90 – 120</b>	3.0	100	$< 1.0$
<b>up to 205</b>	2.0	150	$\sim 2.0$

If the molecular clouds are exposed to UV-radiation which can dissociate the CO molecule,  $\text{C}^{18}\text{O}$  should be more localized in the cloud cores than  $^{12}\text{CO}$  because the self-shielding of the more abundant  $^{12}\text{CO}$  is more effective (see, e.g., Bally & Langer 1982). If so, the  $^{12}\text{CO}/\text{C}^{18}\text{O}$  ratios will be larger in the outer layers of the clouds and, hence, the same intensity ratio corresponds to a higher optical depth in  $^{12}\text{CO}$ . However, this effect should not be large because the UV-radiation field in the Galactic center region, away from Sgr B2, is not intense and a large part of the shielding should be provided by dust. In addition, if this effect is present it should affect high intensity ratios with weak undetected  $\text{C}^{18}\text{O}$  emission the most. Thus, the true ratios in areas where UV dissociation might be important are higher and our use of lower limits tends to deemphasize this “UV-radiation effect”.

So far, we have assumed that the  $^{12}\text{CO}$  and the  $\text{C}^{18}\text{O}$  emission arises in the same volume. However, in a scenario of cool and dense molecular cloud cores surrounded by a

hotter and thinner molecular component Hüttemeister et al. (1993), it is possible that the  $^{12}\text{CO}$  emission originates in part or even completely in the thin component, while the  $\text{C}^{18}\text{O}$  emission arises mostly from these clouds cores. This is the case if the cloud cores are self-shielded in  $^{12}\text{CO}$ . Sgr B2 is, in fact, known to have a hot low density envelope of molecular gas (see, e.g., Hüttemeister et al. 1995). Then, the line intensity of  $^{12}\text{CO}$  is based on higher  $T_{\text{kin}}$  and lower  $n_{\text{H}_2}$  than the line intensity of  $\text{C}^{18}\text{O}$ . To model the resulting line intensity ratio of such a scenario, we used the  $\text{C}^{18}\text{O}$  line intensities of our LVG calculations determined for densities higher by 0.5 dex and for temperatures lower by 50 K compared to the values used for  $^{12}\text{CO}$ . It turns out that, for the range of parameters considered above, the resulting ratios are uniformly low (25–40). The dominating effect in this result is the density gradient which causes a large reduction of the intensity ratio. The temperature gradient causes a slight increase of the intensity ratio which is an opposite but only marginal effect compared to the density gradient. Obviously, such ratios are not compatible with our observations. Therefore, our result that the optical depth of  $^{12}\text{CO}$  is moderate or even low is confirmed and our assumption that the  $^{12}\text{CO}$  and the  $\text{C}^{18}\text{O}$  emission arises in the same volume is justified.

In summary, the LVG calculations confirm that the large scale  $^{12}\text{CO}(1-0)$  emission in the Galactic center region is dominated by emission with intermediate ( $\tau = 1-5$ ) or low optical depths ( $\tau < 1$ ). High optical depth emission ( $\tau \geq 10$ ) commonly found in molecular clouds of the Galactic disk (e.g. Phillips et al. 1979) is restricted to very limited areas such as Sgr B2.

#### 2.4. Estimates of the $\text{H}_2$ Mass from CO Isotopomers

We now estimate the total  $\text{H}_2$  mass of the inner Galactic center region, i.e. the Galactic bulge. From the extent of the  $^{12}\text{CO}(1-0)$  emission (see Fig. 2) the Galactic bulge is assumed to range from  $l = -1^\circ 5$  to  $+2^\circ 25$  and  $b = -0^\circ 75$  to  $+0^\circ 75$ , corresponding to  $555 \text{ pc} \times 220 \text{ pc}$ .

##### 2.4.1. Mass Estimate from the $^{12}\text{CO}$ Standard Conversion Factor

As a first step, the total  $\text{H}_2$  mass is estimated from the  $^{12}\text{CO}(1-0)$  luminosity determined from the data of Bitran (1987). The SCF (Eq. 1) gives the  $\text{H}_2$  column density. To obtain the total  $\text{H}_2$  mass, we have to multiply this result by the mass of a  $\text{H}_2$  molecule and by the area each position represents. This area is given by the spacing of the map, hence,  $0^\circ 125 \times 0^\circ 125$  which corresponds to  $3.274 \cdot 10^{39} \text{ cm}^2$  at 8.5 kpc. Therefore, we obtain:

$$\mathcal{M}_{\text{H}_2}^{12\text{CO}} = \frac{1.27 \cdot 10^3 \text{ M}_\odot}{\text{K km s}^{-1}} \cdot \sum_{\text{positions}} \int T_{\text{MB}}^{12\text{CO}(1-0)}(v) dv \quad (2)$$

The total luminosity of the Galactic bulge in  $^{12}\text{CO}(1-0)$  is  $1.52 \cdot 10^5 \text{ K km s}^{-1}$  where the intensities are integrated over the velocity range from  $-225.0$  to  $+225.0 \text{ km s}^{-1}$  and summed over the area from  $l = -1^\circ 5$  to  $2^\circ 25$  and from  $b = -0^\circ 75$  to  $+0^\circ 75$ . With this we obtain a mass of:

$$\mathcal{M}_{\text{H}_2}^{12\text{CO}}(l=-1.5 \text{ to } +2.25, b=-0.75 \text{ to } +0.75) = 1.93 \cdot 10^8 \text{ M}_\odot \quad (3)$$

##### 2.4.2. Mass Estimate from the $\text{C}^{18}\text{O}$ Data

In the optically thin case, the column density of  $\text{C}^{18}\text{O}$  in the  $J = 0$  state can be determined from the integrated intensity as (see Eq. 14.45 in Rohlfs & Wilson 1996):

$$\bar{\mathcal{N}}_{J=0}^{\text{C}^{18}\text{O}} = \frac{1.21 \cdot 10^{14} \text{ cm}^{-2}}{\text{K km s}^{-1}} \int T_{\text{MB}}^{\text{C}^{18}\text{O}(1-0)} dv \quad (4)$$

The ratio of  $\bar{\mathcal{N}}_{J=0}^{\text{C}^{18}\text{O}}$  to the total column density of  $\text{C}^{18}\text{O}$  can be estimated from LVG calculations if we assume reasonable average values for  $T_{\text{kin}}$  and  $\log(n_{\text{H}_2})$ . Because  $\text{C}^{18}\text{O}(1-0)$  is optically thin, emission from subthermally excited gas is too weak to be seen and  $\log(n_{\text{H}_2})$  is  $\gtrsim 3.0$ . About 60% of the integrated intensity of  $\text{C}^{18}\text{O}$  originates from positions in the  $l, b, v$ -space where the  $^{12}\text{CO}/\text{C}^{18}\text{O}$  ratio is lower than 50. Compared with the components identified in Section 2.3, it seems likely that most of the  $\text{C}^{18}\text{O}$  emission originates in gas with  $\log(n_{\text{H}_2}) \approx 3.5$  (at  $T_{\text{kin}} \approx 50 \text{ K}$  and  $\tau^{12\text{CO}(1-0)} \approx 3.0$ ). This is in good agreement with Hüttemeister (1993), chap. 5, who obtained  $\log(n_{\text{H}_2}) \gtrsim 3.7$  for  $\text{C}^{18}\text{O}$  emission toward CS(2-1) peak positions. For these values the LVG calculations with the appropriate velocity gradients give  $\bar{\mathcal{N}}^{\text{C}^{18}\text{O}} \approx 6.5 \cdot \bar{\mathcal{N}}_{J=0}^{\text{C}^{18}\text{O}}$ . This value varies by a factor of 2 if the density is modified to  $\log(n_{\text{H}_2}) = 3.0$  or  $4.0$  or if  $T_{\text{kin}}$  is increased. To obtain the total  $\text{H}_2$  mass from  $\bar{\mathcal{N}}^{\text{C}^{18}\text{O}}$ , we take  $\text{C}^{18}\text{O}/\text{H}_2 = 4 \cdot 10^{-7}$  (i.e.  $^{12}\text{CO}/\text{H}_2 = 10^{-4}$ ), and then carry out the same steps as for  $^{12}\text{CO}$ . Because the spacing of the map was  $9'$  instead of  $7.5'$ , the area each position represents is  $0^\circ 15 \times 0^\circ 15 \hat{=} 4.715 \cdot 10^{39} \text{ cm}^2$ . Therefore, the total  $\text{H}_2$  mass is given by:

$$\mathcal{M}_{\text{H}_2}^{\text{C}^{18}\text{O}} = \frac{1.56 \cdot 10^4 \text{ M}_\odot}{\text{K km s}^{-1}} \cdot \sum_{\text{positions}} \int T_{\text{MB}}^{\text{C}^{18}\text{O}(1-0)}(v) dv \quad (5)$$

With the luminosity of  $\text{C}^{18}\text{O}(1-0)$  being  $745 \text{ K km s}^{-1}$  where the intensities are integrated over the same velocity range as  $^{12}\text{CO}$  and summed over the area from  $l = -1^\circ 05$  to  $2^\circ 25$  and from  $b = -0^\circ 75$  to  $+0^\circ 75$ , we find a total  $\text{H}_2$  mass of:

$$\mathcal{M}_{\text{H}_2}^{\text{C}^{18}\text{O}}(l=-1.05 \text{ to } +2.25, b=-0.75 \text{ to } +0.75) = 1.16 \cdot 10^7 \text{ M}_\odot \quad (6)$$

This value is more than an order of magnitude less than that determined by the SCF from  $^{12}\text{CO}(1-0)$ . It is also lower than the “weighted guess” of about  $0.8 \cdot 10^8 \text{ M}_\odot$

compiled by Güsten (1989) from a collection of several observations (see also Section 3.1).

However, we must take into account that there might be a considerable contribution to the molecular mass from  $\text{C}^{18}\text{O}$  emission which is below our detection limit (see Section 2.2). To determine an upper limit, we determine the luminosity of  $\text{C}^{18}\text{O}(1-0)$  with a  $1\sigma$ -threshold which gives us the absolute upper limit allowed by the data. Certainly, the luminosity of  $\text{C}^{18}\text{O}(1-0)$  is expected to be lower because the intensity of  $\text{C}^{18}\text{O}$  is not everywhere as high as  $1\sigma$  where it is not detected. To avoid areas with *no* molecular gas, we use the presence of  $^{12}\text{CO}$  emission as a constraint for the integration range in  $\text{C}^{18}\text{O}$ . As mentioned in Section 6.2.2 of Paper I, the  $^{12}\text{CO}$  emission has a constant velocity width of about  $375 \text{ km s}^{-1}$ , the central velocity of which can be described by the relation with  $v_{\text{center}}(l) = l \cdot 41.4 \text{ km s}^{-1}/\text{arcdeg} + 7.2 \text{ km s}^{-1}$  for  $l \leq 2^\circ 0$  and  $v_{\text{center}}(l) = 90.0 \text{ km s}^{-1}$  for  $l > 2^\circ 0$ . With this, the upper limit of the  $\text{C}^{18}\text{O}(1-0)$  luminosity is  $4100 \text{ K km s}^{-1}$ . Then, the upper limit of the total  $\text{H}_2$  mass from  $\text{C}^{18}\text{O}(1-0)$  emission allowed by the data is:

$$\mathcal{M}_{\text{H}_2}^{\text{C}^{18}\text{O}}(l=-1.05 \text{ to } +2.25, b=-0.75 \text{ to } +0.75) < 6.41 \cdot 10^7 M_\odot \quad (7)$$

Even this limit is a factor of 3 lower than the total  $\text{H}_2$  mass determined with the SCF and still slightly lower than the “weighted guess” by Güsten (1989).

A larger  $^{12}\text{CO}/\text{C}^{18}\text{O}$  ratio due to selective UV dissociation of  $\text{C}^{18}\text{O}$  would increase  $\mathcal{M}_{\text{H}_2}^{\text{C}^{18}\text{O}}$  linearly; conversely a  $^{12}\text{CO}/\text{H}_2$  ratio  $> 10^{-4}$  due to higher metallicity in the Galactic center would decrease *all* masses derived from CO isotopomers. For example, Irvine et al. (1985) find  $5 \cdot 10^{-4}$  in the envelope of the evolved carbon star IRC+10216 and Arimoto et al. (1996) derive metallicity-dependent CO-to- $\text{H}_2$  conversion factors. Both effects might add an uncertainty of a factor of  $\sim 2$  to the  $\mathcal{M}_{\text{H}_2}^{\text{C}^{18}\text{O}}$  mass, but will cause changes in opposite directions. Considering that the scaling of  $\bar{\mathcal{N}}_{J=0}^{\text{C}^{18}\text{O}}$  to  $\bar{\mathcal{N}}^{\text{C}^{18}\text{O}}$  is also uncertain by about a factor of 2, we estimate that the  $\mathcal{M}_{\text{H}_2}^{\text{C}^{18}\text{O}}$  is uncertain by a factor of  $\sim 3$ . Thus, it is formally possible (but unlikely) to raise the upper limit of  $\mathcal{M}_{\text{H}_2}^{\text{C}^{18}\text{O}}$  allowed by the data sufficiently to be consistent with the mass obtained from  $^{12}\text{CO}$  by the SCF. However, because this formal upper limit is for sure significantly larger than the true value, any consistency with the SCF can be ruled out.

### 2.4.3. The Thin Gas Contribution

We find a molecular gas component with low  $\text{H}_2$  densities and high kinetic temperatures to be widespread in agreement with Oka et al. (1997). In this component, the CO level populations are likely to be subthermal, as indicated by the high  $^{12}\text{CO}/\text{C}^{18}\text{O}$  ratio and the LVG calculations. In this case, emission of  $\text{C}^{18}\text{O}$  is very difficult to detect since the subthermal excitation is correlated with low

gas densities and low column densities. Indeed about 60% of the  $\text{C}^{18}\text{O}$  emission originates in  $l, b, v$ -channels where the  $^{12}\text{CO}/\text{C}^{18}\text{O}$  ratio is below 50 whereas only 10% of it originate in  $l, b, v$ -channels where the  $^{12}\text{CO}/\text{C}^{18}\text{O}$  ratio is above 90. The non-detection of  $\text{C}^{18}\text{O}$  places a limit on the possible  $\text{H}_2$  column density (and mass) in this region (see above). Using the physical conditions given by the LVG-model for high  $^{12}\text{CO}/\text{C}^{18}\text{O}$  ratios, we can achieve a better estimate of the (possibly significant) contribution of this “thin gas component” missing from the  $\text{C}^{18}\text{O}$  mass budget.

We assume that the  $^{12}\text{CO}$  emission which appears at positions in the  $l, b, v$ -space where no  $\text{C}^{18}\text{O}$  emission is detected originates in the thin gas component. This criterion is reasonable but not without problems, since (1) some thermalized  $\text{C}^{18}\text{O}$  emission might be present below our detection limit and (2) even if we detect  $\text{C}^{18}\text{O}$ , it is not guaranteed that *all* the  $^{12}\text{CO}$  emission originates in thermalized molecular gas from which the  $\text{C}^{18}\text{O}$  emission arises. However, our LVG calculations predict subthermal excitation conditions in regions of high  $^{12}\text{CO}/\text{C}^{18}\text{O}$  ratios and moderate optical depths. As discussed above, this excludes that  $^{12}\text{CO}$  emission from hot, low density gas can shield the dense cores completely.

In estimating the mass of the thin gas component, we considered the complete range of emission from  $-225 \text{ km s}^{-1}$  to  $+225 \text{ km s}^{-1}$  for  $^{12}\text{CO}$  and restricted the integration to positions in the  $l, b, v$ -space where the  $\text{C}^{18}\text{O}$  emission is below  $2\sigma_{\text{C}^{18}\text{O}}$ , i.e. below  $0.072 \text{ K}$ . This procedure required the  $^{12}\text{CO}$  data to be sampled on the same grid in the  $l, b, v$ -space as the  $\text{C}^{18}\text{O}$  data. Thus, the data cube with the  $^{12}\text{CO}$  data of Bitran (1987) resampled to the slightly lower velocity and spatial resolution of the  $\text{C}^{18}\text{O}$  spectra (see Section 2.2) was used. From this, the  $^{12}\text{CO}$  luminosity of areas where the  $\text{C}^{18}\text{O}$  emission is too weak to be detected is  $7.78 \cdot 10^4 \text{ K km s}^{-1}$ . This is roughly 1/2 of the total luminosity of  $^{12}\text{CO}$ . Because we expect the optical depth of  $^{12}\text{CO}$  to be moderate ( $\tau_0 \lesssim 1$ ) but not  $\ll 1$ , we use the approximation

$$f_{\text{beam}} T_{\text{ex}} \int \tau(v) dv \cong \frac{\tau_0}{1 - e^{-\tau_0}} \int T_{\text{MB}}(v) dv \quad (8)$$

which is accurate to 15% for  $\tau_0 < 2$ , and it always overestimates  $\bar{\mathcal{N}}$  when  $\tau_0 > 1$  (Rohlfs & Wilson 1996). Then, we obtain for the column density of  $^{12}\text{CO}$  in the state  $J = 0$ :

$$\bar{\mathcal{N}}_{J=0}^{12\text{CO}_{\text{thin}}} = \frac{1.15 \cdot 10^{14} \text{ cm}^{-2}}{\text{K km s}^{-1}} \cdot \frac{\tau_0^{12\text{CO}(1-0)}}{1 - e^{-\tau_0^{12\text{CO}(1-0)}}} \int T_{\text{MB}}^{12\text{CO}(1-0)} dv \quad (9)$$

Assuming  $T_{\text{kin}} \approx 150.0 \text{ K}$  and  $n_{\text{H}_2} \approx 10^{2.5} \text{ cm}^{-3}$  as a good approximation to the hot low density component, the LVG calculations (Section 2.3) yield  $\bar{\mathcal{N}}^{12\text{CO}_{\text{thin}}} \approx 5.75 \cdot \bar{\mathcal{N}}_{J=0}^{12\text{CO}_{\text{thin}}}$  and  $\tau_0^{12} / (1 - \exp(-\tau_0^{12})) \approx 1.78$ . Assuming

**Table 2.** The gas mass in the central 600 pc of the Galactic center from different tracers

Tracer	$\mathcal{M}_{\text{mol}}$	Reference
$^{12}\text{CO}(1-0)$ (SCF)	$2.8 \cdot 10^8 M_{\odot}$	This work, Eq. 3 <sup>a</sup>
$\text{C}^{18}\text{O}(1-0)$	$1.7 \cdot 10^7 M_{\odot}$	This work, Eq. 6 <sup>a</sup>
$^{12}\text{CO}(1-0)$ (thin gas)	$\sim 1.0 \cdot 10^7 M_{\odot}$	This work, Eq. 11 <sup>a</sup>
Dust / IRAS	$3.6 \cdot 10^7 M_{\odot}$	Cox & Laureijs (1989)
Dust 800 $\mu\text{m}$	$> 0.4 \cdot 10^7 M_{\odot}$	Lis & Carlstrom (1994)
Dust / COBE	$3.1 - 7.0 \cdot 10^7 M_{\odot}$	Sodroski et al. (1994) / data of Bitran (1987) <sup>a</sup>
0.1–1.0 GeV $\gamma$ -rays	$< 5.8 \cdot 10^7 M_{\odot}$	Blitz et al. (1985)

<sup>a</sup> Divided by 0.7 to take into account that only 70% of the total mass is found in hydrogen.

again a  $^{12}\text{CO}/\text{H}_2$  ratio of  $10^{-4}$ , the  $\text{H}_2$  mass is:

$$\mathcal{M}_{\text{H}_2}^{12\text{COthin}} = \frac{93.8 M_{\odot}}{\text{K km s}^{-1}} \cdot \sum_{\text{positions}} \int T_{\text{MB}}^{12\text{CO}(1-0)}(v) dv \quad (10)$$

Comparing this equation with Eq. 2, it is obvious that in case of low or intermediate optical depth the same  $^{12}\text{CO}(1-0)$  luminosity corresponds to an  $\text{H}_2$  mass which is more than an order of magnitude lower. With the above estimate of the  $^{12}\text{CO}(1-0)$  luminosity of the “thin gas component” we determine:

$$\mathcal{M}_{\text{H}_2}^{12\text{COthin}} \left( \begin{smallmatrix} l=-1.05 \text{ to } +2.25 \\ b=-0.75 \text{ to } +0.75 \end{smallmatrix} \right) = 0.73 \cdot 10^7 M_{\odot} \quad (11)$$

This is  $\sim 60\%$  of the mass determined from  $\text{C}^{18}\text{O}$ .

This mass will be larger if the portion of  $^{12}\text{CO}$  emission which originates in thin gas is higher, or if the  $^{12}\text{CO}/\text{H}_2$  ratio in this component is lower than  $10^{-4}$ , because of less effective shielding in low-density gas, leading to enhanced CO dissociation. Thus, we estimate that the molecular mass in the thin gas component might be as high as twice the value calculated. Therefore, this component may contain as much gas as the denser and cooler cloud cores traced by  $\text{C}^{18}\text{O}$ .

### 3. Discussion

#### 3.1. The Molecular Mass in the Galactic Bulge

##### 3.1.1. Mass Estimates from other Tracers

To better assess the uncertainties of our total molecular mass estimate, we compare the values obtained from CO data with results obtained from other tracers.

Cox & Laureijs (1989) analyzed IRAS data of thermal dust emission in the inner 500 pc of the Galactic Center. Using  $T_{\text{dust}} = 27$  K and a metallicity  $Z = 2 Z_{\odot}$ , they found a total gas mass of  $3.6 \cdot 10^7 M_{\odot}$ .

Lis & Carlstrom (1994) presented an 800  $\mu\text{m}$  survey of the inner  $1.5 \times 0.2$  which is sensitive to cooler dust than IRAS. However, due to a small chopper amplitude, their estimate is limited to small scale structure. They determined a lower limit to the total gas mass of  $0.4 \cdot 10^7 M_{\odot}$ .

One half of this mass arises from the Sgr B2 region. From the mass determined from  $\text{C}^{18}\text{O}$ , we estimate that Lis & Carlstrom recorded about 25% of the total gas in the region mapped and about 50% toward Sgr B2. When compared to our data, we find that the distribution of the dust is better correlated with the  $\text{C}^{18}\text{O}$  emission than with the  $^{12}\text{CO}$  emission, especially near Sgr B2.

In an analysis of Galactic plane surveys from the Diffuse Infrared Background Experiment (DIRBE) of the Cosmic Background Explorer (COBE) at 140  $\mu\text{m}$  and 240  $\mu\text{m}$ , Sodroski et al. (1994) obtained dust-to-gas ratios ( $d/g$ ) along the Galactic plane. If one assumes a unique  $I_{\text{CO}}/\mathcal{N}_{\text{H}_2}$  conversion factor and compares dust emission to  $^{12}\text{CO}$  and HI data, one finds that the ratio in the inner  $4^\circ$ , i.e. the Galactic bulge, decreases by a factor of 2 – 3 relative to the inner disk. The dust-to-gas ratio also depends on metallicity (Mezger et al. 1986) which is 2 – 3 times higher in the Galactic bulge than in the inner disk (Cox & Laureijs 1989). Then, the dust-to-gas ratio in the Galactic bulge would actually be lower by a factor 4 – 9 than in the disk. Sodroski et al. (1994) proposed that the  $\mathcal{N}_{\text{H}_2}/I_{\text{CO}}$  ratio is also lower by a factor of 4 – 9. Using this conversion factor, we obtain a total  $\text{H}_2$  mass of  $2.2$  to  $4.9 \cdot 10^7 M_{\odot}$  from the  $^{12}\text{CO}(1-0)$  data of Bitran (1987), in good agreement with our  $\text{C}^{18}\text{O}$  result.

An independent mass estimate based on  $\gamma$ -rays from 0.1 GeV to 1.0 GeV that are produced when cosmic rays interact with the interstellar gas (Blitz et al. 1985) gives an upper limit to the gas mass of the Galactic bulge of  $5.8 \cdot 10^7 M_{\odot}$ . However, Silk & Bloemen (1987) found that the  $\gamma$ -ray flux in the range from 1 GeV to 5 GeV is compatible with the  $^{12}\text{CO}(1-0)$  luminosity and the SCF if the cosmic-ray density ( $> 1$  GeV) is the same as that found in the Galactic plane by Bloemen et al. (1986).

##### 3.1.2. A Weighted Best Estimate

In Table 2, we summarize the values for the total molecular mass in the Galactic bulge from different tracers. The estimates of the total mass in the molecular phase based on dust and on  $\text{C}^{18}\text{O}$  agree reasonably well, especially if one takes the thin gas component into account. The  $^{12}\text{CO}$  data yield a much higher mass if the SCF is used.

The previous weighted guess was  $8 \cdot 10^7 M_\odot$  (Güsten 1989), including the mass determined from  $^{12}\text{CO}$  with the SCF. There is now additional evidence for an even lower mass, from our  $\text{C}^{18}\text{O}$  data and the COBE data presented by Sodroski et al. (1994). In addition, we have shown that the SCF *cannot* be applied to the Galactic center region (see also next section). Therefore, our *weighted best estimate* for the molecular mass in the Galactic bulge is:

$$\mathcal{M}_{\text{mol}} = (3_{-1}^{+2}) \cdot 10^7 M_\odot \quad (12)$$

The errors include the results of mass determinations from  $\text{C}^{18}\text{O}$  data,  $\gamma$ -ray flux, and dust emission, but exclude the  $^{12}\text{CO}$  SCF value. They are also compatible with an additional hot low density component of similar mass as the gas traced by  $\text{C}^{18}\text{O}$ .

### 3.2. The $^{12}\text{CO}$ Conversion Factor toward the Galactic Bulge

We have shown that the SCF gives a column density of molecular hydrogen,  $\bar{\mathcal{N}}_{\text{H}_2}$ , that is too high by an order of magnitude in the Galactic bulge. This may have far-reaching consequences for the interpretation of galactic and extragalactic data and, hence, warrants a more detailed investigation.

The SCF, obtained by Strong et al. (1988), is based on two major assumptions: a) the emission of  $^{12}\text{CO}(1-0)$  is optically thick and b) the molecular clouds are virialized. A comparison of Eq. A5 for  $\bar{\mathcal{N}}_{12\text{CO}}$  in case of intermediate and low optical depths with Eq. 1 (assuming  $^{12}\text{CO}/\text{H}_2 = 10^{-4}$ ) for  $\bar{\mathcal{N}}_{12\text{CO}}$  in the optically thick case (SCF) shows that if one erroneously assumes optically thick  $^{12}\text{CO}$  emission and applies the SCF (Eq. 1), one overestimates the total  $\text{H}_2$  mass,  $\mathcal{M}_{\text{H}_2}$ , by a factor of up to 80. This illustrates that only a few percent of  $^{12}\text{CO}$  molecules emitting under optically thin conditions can contribute a large fraction of the  $^{12}\text{CO}$  luminosity and, hence, strongly influence the estimates of gas masses. Therefore, the areas of low or intermediate optical depth, that dominate the  $^{12}\text{CO}$  emission in the Galactic center over large scales, are at least partly responsible for the overestimation of the molecular mass by the SCF.

One reason for the anomalously low optical depths of the  $^{12}\text{CO}$  emission are the large linewidths of Galactic center clouds which are an order of magnitude larger than those found for disk Giant Molecular Clouds (GMCs). Thus, the optical depths per column density are an order of magnitude lower in the Galactic Center than in Galactic disk clouds.

Furthermore, the assumption that the molecular clouds are virialized may be not fulfilled in many cases. Molecular clouds can only be virialized if their mean density,  $n_{\text{H}_2}$ , exceeds  $10^4 \text{ cm}^{-3}$  ( $75 \text{ pc} / D_{\text{GC}}$ )<sup>1,8</sup> where  $D_{\text{GC}}$  is the distance from the Galactic center (see, e.g., Güsten & Downes 1980). Therefore, the densities must be  $2000 - 5000 \text{ cm}^{-3}$  in the outer bulge ( $D_{\text{GC}} > 100 \text{ pc}$ ) and

$10000 \text{ cm}^{-3}$  and more in the inner bulge ( $D_{\text{GC}} < 100 \text{ pc}$ ) to be stable. Since  $\text{C}^{18}\text{O}$  is collisionally excited and, thus, detectable at these densities, we expect that the molecular gas in virialized clouds is traced completely by  $\text{C}^{18}\text{O}$  emission. With a mean density of the gas emitting  $\text{C}^{18}\text{O}$  of about  $3000 \text{ cm}^{-3}$ , the dense cores (which are the strongest sources in  $\text{C}^{18}\text{O}$ ) should indeed be virialized. This is supported by the fact that mass estimates based on the SCF are closer to the  $\text{C}^{18}\text{O}$  masses toward molecular peaks: *Globally* the discrepancy is about a factor of 16, dropping to 5–6 for Sgr B2 and Sgr A, and becoming even smaller when the peaks are investigated with higher angular resolution (see, e.g., Mauersberger et al. 1989).

For non-virialized gas, the  $^{12}\text{CO}$  line width traces not the molecular mass of the cloud but the dynamical mass which causes the gravitational potential the molecular cloud is moving through. Downes et al. (1993) find that the standard conversion factor overestimates the true gas mass by a factor of  $\sqrt{\mathcal{M}_{\text{stars}}/\mathcal{M}_{\text{H}_2}}$  if the average stellar mass density exceeds the gas mass density. With  $<1\%$  of the mass of the Galactic bulge in the gas phase (see, e.g., Güsten 1989), the mass determined from the  $^{12}\text{CO}$  emission with the SCF should be too high by a factor 10, i.e. the true value should be  $2.8 \cdot 10^7 M_\odot$ , in agreement with the weighted best estimate derived in Section 3.1 if all the molecular gas is located in non-virialized clouds. However, such a scenario implies that all the molecular gas fulfills the other precondition of the SCF, namely that the  $^{12}\text{CO}$  emission is optically thick. From our LVG calculations, this is not the case. Thus, a significant part of the dense cores, containing a major fraction of the total mass, must be virialized even though the virialization density is rather high, in particular higher than the thermalization density. Therefore, the non-virialization of molecular clouds is an important but not the only reason for the overestimate of the molecular mass from the  $^{12}\text{CO}$  luminosity by the SCF. On the other hand, the fact that, nearly everywhere in the Galactic center region, the virialization density is higher than the thermalization density implies that the unbound gas cannot simply be identified with the “thin gas” component discussed above.

In summary, the  $^{12}\text{CO}$  luminosity is larger than predicted by the SCF since:

- (1) The  $^{12}\text{CO}$  emission on large scales is dominated by lines that are not optically thick.
- (2) A considerable fraction of the gas is not virialized.

Both effects tend to affect the same gas component, and we stress that the main cause of the difference in mass estimates from the two CO isotopomers is not the emission from the peaks but the extended emission from  $^{12}\text{CO}$  of rather low optical depth, in particular the hot low density component (thin gas). Therefore, it is *not* correct just to apply a modified conversion factor to the Galactic center region as done by Arimoto et al. (1996) and Oka et al. (1997). The point is that in the Galactic center region

the  $^{12}\text{CO}$  luminosity has *no* direct causal connection with the molecular mass. This is shown by the different line shapes of  $^{12}\text{CO}(1-0)$  and  $\text{C}^{18}\text{O}(1-0)$  (Fig. 3) and by the large variation of the  $^{12}\text{CO}/\text{C}^{18}\text{O}$  ratio (Fig. 5).

### 3.3. Consequences for other Galactic Nuclei

In our Galaxy, the Galactic center is a unique object displaying many features not present in the Galactic disk. Thus, large scale physics and properties found in detailed investigations of our Galactic center region should be compared to central regions of other galaxies, especially of spirals similar to ours.

#### 3.3.1. A Comparison with IC 342

The late-type spiral galaxy IC 342 is thought to be similar to the Milky Way. For our comparison, we use the  $^{12}\text{CO}(1-0)$  observations of the central region in IC 342 obtained by Ishizuki et al. (1990) with the Nobeyama Millimeter Array (NMA). The map has an angular resolution of  $2''.4$ , corresponding to 22.5 pc at a distance to IC 342 of 1.85 Mpc (McCall 1989), which is identical to the linear resolution of our  $\text{C}^{18}\text{O}$  and  $^{12}\text{CO}$  data. The extent of its central region is  $62''.5 \times 37''.1$  (560 pc  $\times$  335 pc), very close to the size of our Galactic bulge.

From Fig. 2(a) of Ishizuki et al. (1990), the molecular gas traces two narrow ridges which form a small-scale spiral in the bulge and are associated with shock waves. Molecular condensations of similar structure and extent as Sgr A, Sgr B2, Sgr C or the 1.5-complex (Sgr D region) can be recognized. From the SCF, Ishizuki et al. determine the molecular mass of the central region of IC 342 as  $2.6 \cdot 10^8 M_{\odot}$ . If, however, the mass in IC 342 determined by this factor is as greatly overestimated as in the Galactic center region, the true molecular mass of IC 342 should be  $\sim 2.8 \cdot 10^7 M_{\odot}$ , nearly the same as the weighted best estimate for our Galactic bulge.

In a detailed analysis of the central region of IC 342 based on the high density tracer  $\text{HCN}(1-0)$  and  $^{12}\text{CO}$  (Ishizuki et al. 1990),  $^{13}\text{CO}$  (Ishizuki et al. 1991; Turner & Hurt 1992) and  $\text{NH}_3$  (Ho et al. 1990) data, Downes et al. (1992) concluded that the  $^{12}\text{CO}$  and  $^{13}\text{CO}$  emission does not trace the same material, postulating at least three gas components: low density gas at  $150 - 300 \text{ cm}^{-3}$  accounts for most of the  $^{12}\text{CO}$ , moderate density gas at  $500 - 3000 \text{ cm}^{-3}$  for the  $^{13}\text{CO}$  and high density cores  $\gtrsim 10^4 \text{ cm}^{-3}$  for the  $\text{HCN}$ . From  $\text{NH}_3$ , the kinetic temperature for moderate and high densities is  $50 - 70 \text{ K}$ . This picture closely resembles our results for the Galactic center region (see this paper for the low and moderate density component; high density cores traced by the CS survey of Bally et al. (1987) are investigated in detail by Hüttemeister (1993), chapt. 5;  $\text{NH}_3$  observations are described in Hüttemeister et al. (1993)).

However, Downes et al. (1992) stated, without reference to method, that the low density gas should have rather low kinetic temperatures of  $\sim 30 \text{ K}$ . But low density gas cools less effectively than denser material that, in addition to cooling by line radiation, can transfer energy to dust grains more easily because it is better coupled to dust grains by collisions. Therefore, the thin gas which should be heated strongly by shocks is more likely to have higher kinetic temperatures than the denser gas component, as it is found for our Galactic center region.

#### 3.3.2. The Starburst Galaxy NGC 253

In contrast to the rather quiescent state of our Galaxy and of IC 342, the nearly edge-on spiral galaxy NGC 253 ( $i = 78^\circ$ , Pence 1981) is a good example for a nuclear starburst (Rieke et al. 1988). The molecular distribution and mass of this nearby ( $D = 2.5 \text{ Mpc}$ ) galaxy was investigated in detail by Mauersberger et al. (1996). They found that the molecular gas mass in the central condensations of NGC 253 is also overestimated from an application of the SCF. They determined a mass of about  $5 \cdot 10^7 M_{\odot}$  from  $\text{C}^{18}\text{O}$  lines and mm-wave dust continuum for the central 300 pc whereas the SCF yields a result which is higher by a factor of  $\sim 6$ . They conclude that the SCF cannot be applied to the central region of NGC 253 for the same reasons we found for our Galactic center region.

This mass determination is confirmed by Paglione et al. (1995) who investigated dense clouds in the central region of NGC 253 in the  $\text{HCN}(1-0)$  line using the Nobeyama Millimeter Array (NMA). From molecular excitation models, they found a total mass of molecular gas within the central 400 pc of  $1.4 \cdot 10^8 M_{\odot}$ , in good agreement with Mauersberger et al. (1996) who determined  $1.3 \cdot 10^8 M_{\odot}$ .

#### 3.3.3. Other Galaxies

For IC 694 and the mergers NGC 1614 and Arp 220, Shier et al. (1994) argued that the SCF cannot be applied to the central regions. They determined the total mass present in the central regions and found in all three galaxies that the  $\text{H}_2$  masses derived from the SCF are higher than the total mass including stars which is obviously impossible. Together with the results previously mentioned and our result for the central region of our Galaxy, this shows that the non-applicability of the SCF is probably a general property of the central region of galaxies.

The existence of a hot low density gas component in the central region was also favored by Aalto et al. (1995) for a sample of 32 external galaxies consisting of starburst galaxies, interacting galaxies and two quiescent systems. From their single-dish observations Aalto et al. concluded that most of the  $^{12}\text{CO}$  emission originates in this low density component, under conditions of only moderate optical depth, and found  $^{12}\text{CO}/\text{C}^{18}\text{O}$  ratios that are significantly

above the values in the disk of the Milky Way, although not as high as the most extreme ratios found for our Galactic Center region. However, this is readily explained by the fact that their beam averages over the dense and the thin component, while the different components are at least partly resolved toward the Galactic center region. This indicates that the existence of a hot low density gas component which dominates the  $^{12}\text{CO}$  emission is also very likely to be a general property of the central region of galaxies.

#### 4. Conclusions

From the large scale  $\text{C}^{18}\text{O}(1-0)$  Galactic Center Survey, presented in Paper I, we obtain the following results:

- (1) In the Galactic center region, the standard conversion factor (SCF) of Strong et al. (1988) which relates the  $\text{H}_2$  column density to the integrated intensity of the  $^{12}\text{CO}(1-0)$  line,  $I_{12\text{CO}}$ , is *not* valid. The SCF overestimates  $\mathcal{N}_{\text{H}_2}$  by a factor of  $\sim 9$ . This overestimate is caused by the high luminosity of  $^{12}\text{CO}$  lines of moderate and low optical depth from a rather small but widespread fraction of the gas and the non-virialization of a considerable fraction of the molecular gas in the gravitational potential of the Galactic center region. Therefore, also one can not apply a modified conversion factor to the Galactic center region since the  $^{12}\text{CO}$  luminosity is not connected in a direct way with molecular mass. In particular, this is shown by the different line shapes of  $^{12}\text{CO}(1-0)$  and  $\text{C}^{18}\text{O}(1-0)$  and by the large variation of the  $^{12}\text{CO}/\text{C}^{18}\text{O}$  integrated intensity ratio.
- (2) The integrated intensity ratio of  $^{12}\text{CO}/\text{C}^{18}\text{O}$  in the Galactic Center region is generally higher than the value of about 15 which is expected from the “standard” conversion factors. In the  $9'$ -beam, this ratio is at least of the order 40, mostly of the order of 60 to 80, in several  $l, b, v$ -areas of the order 90 to 120, and toward a few positions up to  $> 200$ .
- (3) From LVG calculations, we find that the large scale  $^{12}\text{CO}$  emission in the Galactic Center region is dominated by emission with intermediate ( $\tau = 1-5$ ) or low optical depths ( $\tau < 1$ ). High optical depth emission ( $\tau \geq 10$ ) is restricted to very limited areas such as Sgr B2. Specifically, we find the following conditions:
  - (a) For  $^{12}\text{CO}/\text{C}^{18}\text{O}$  integrated intensity ratios,  $\lesssim 40$ :  
 $n_{\text{H}_2} \sim 10^{3.5} \text{ cm}^{-3}$ ,  $T_{\text{kin}} \sim 50 \text{ K}$ ,  $\tau \sim 3.0$
  - (b) For the most common ratios, 60 to 80:  
 $n_{\text{H}_2} \sim 10^{3.0} \text{ cm}^{-3}$ ,  $T_{\text{kin}} \sim 50 \text{ K}$ ,  $\tau < 2.0$
  - (c) For high ratios, 90 to 120, found, e.g., in the Sgr D region and Clump 2:  
 $n_{\text{H}_2} \sim 10^{3.0} \text{ cm}^{-3}$ ,  $T_{\text{kin}} \sim 100 \text{ K}$ ,  $\tau < 1.0$
  - (d) For very high ratios up to 200:  
 $n_{\text{H}_2} \sim 10^{2.0} \text{ cm}^{-3}$ ,  $T_{\text{kin}} \sim 150 \text{ K}$ ,  $\tau \sim 2.0$
- (4) We estimate the total molecular mass of the Galactic bulge based on our  $\text{C}^{18}\text{O}$  data, on the  $^{12}\text{CO}$  data of Bitran (1987), and on dust measurements. A molecular gas component of low density (thin gas component) contributes a probably considerable amount of molecular mass. The *weighted best estimate* for the total molecular mass is  $\mathcal{M}_{\text{mol}} = (3_{-1}^{+2}) \cdot 10^7 M_{\odot}$ .
- (5) The lack of a universal  $\mathcal{N}_{\text{H}_2}/I_{12\text{CO}}$  conversion constant and the presence of a mixture of thin and warm gas with cold and dense gas are likely to be general characteristics of the central regions of galaxies.

*Acknowledgements.* We thank Leonardo Bronfman who has made available to us the  $^{12}\text{CO}$  data of Bitran (1987) in digital form before publication. Christian Henkel has kindly provided the LVG radiative transfer program. RM was supported by a Heisenberg fellowship from the Deutsche Forschungsgemeinschaft.

#### References

- Aalto, S., Booth, R.S., Black, J.H., Johansson, L.E.B., 1995, A&A 300, 369
- Arimoto, N., Sofue, Y., Tsujimoto, T., 1996, PASJ 48, 275
- Bally, J., Langer, W.D., 1982, ApJ 255, 143
- Bally, J., Stark, A.A., Wilson, R.W., Henkel, C., 1987, ApJS 65, 13
- Bally, J., Stark, A.A., Wilson, R.W., Henkel, C., 1988, ApJ 324, 223
- Bania, T.M., 1977, ApJ 216, 381
- Bania, T.M., 1980, ApJ 242, 95
- Bania, T.M., 1986, ApJ 308, 868
- Bitran, M.E., 1987, Ph.D. thesis, University of Florida
- Bitran, M.E., Alvarez, H., Bronfman, L., May, J., Thaddeus, P., 1997, A&AS, 124, 1
- Blitz, L., Bloemen, J., Hermsen, W., Bania, T.M., 1985, A&A 143, 267
- Bloemen, J.B.G.M., Strong, A.W., Blitz, L., Cohen, R.S., Dame, T.M., Grabelsky, D.A., Hermsen, W., Lebrun, F., Mayer-Hasselwander, H.A., Thaddeus, P., 1986, A&A 154, 25
- Cox, P., Laureijs, R., 1989, *IRAS Observations of the Galactic Center*. In M. Morris (ed.), *The Center of the Galaxy*, IAU Symp. 136, 121
- Dahmen, G., 1995, Dissertation, Universität Bonn
- Dahmen, G., Hüttemeister, S., Wilson, T.L., Mauersberger, R., Linhart, A., Bronfman, L., Tieftrunk, A.R., Meyer, K., Wiedenhöfer, W., Dame, T.M., Palmer, E.S., May, J., Aparici, J., Mac-Auliffe, F., 1996, *The Molecular Gas in the Galactic Center Region based on  $\text{C}^{18}\text{O}$  Measurements*. In R. Gredel (ed.), *The Galactic Center*, Proceedings of the 4<sup>th</sup> ESO/CTIO Workshop, ASP Conference Series 102, p. 54
- Dahmen, G., Hüttemeister, S., Wilson, T.L., Mauersberger, R., Linhart, A., Bronfman, L., Tieftrunk, A.R., Meyer, K., Wiedenhöfer, W., Dame, T.M., Palmer, E.S., May, J., Aparici, J., Mac-Auliffe, F., 1997 (Paper I), A&AS, 125, 1
- Dame, T.M., 1993, *The Distribution of Neutral Gas in the Milky Way*. In S.S. Holt, F. Verter (eds.), *Back to the Galaxy*, AIP Conference Proceedings 278, p. 267
- de Jong, T., Chu, S.-I., Dalgarno, A., 1975, ApJ 199, 69
- Dickman, R.L., 1975, ApJ 202, 50
- Dickman, R.L., Snell, R.L., Schloerb, F.P., 1986, ApJ 309, 326



- Downes, D., Radford, S.J.E., Guilloteau, S., Guélin, M., Greve, A., Morris, M., 1992, *A&A* 262, 424
- Downes, D., Solomon, P.M., Radford, S.J.E., 1993, *ApJ* 414, L13
- Flower, D.R., Pineau des Forêts, G., Walmsley, C.M., 1995, *A&A* 294, 814
- Green, S., Chapman, S., 1978, *ApJS* 37, 169
- Güsten, R., 1989, *Gas and Dust in the inner few Degrees of the Galaxy*. In M. Morris (ed.), *The Center of the Galaxy*, IAU Symp. 136, 89
- Güsten, R., Downes, D., 1980, *A&A* 87, 6
- Henkel, C., 1980, Dissertation, Universität Bonn
- Ho, P.T.P., Martin, R.N., Turner, J.L., Jackson, J.M., 1990, *ApJ* 355, L19
- Hüttemeister, S., 1993, Dissertation, Universität Bonn
- Hüttemeister, S., Wilson, T.L., Bania, T.M., Martín-Pintado, J., 1993, *A&A* 280, 255
- Hüttemeister, S., Wilson, T.L., Mauersberger, R., Lemme, C., Dahmen, G., Henkel, C., 1995, *A&A* 294, 667
- Hüttemeister, S., Dahmen, G., Mauersberger, R., Henkel, C., Wilson, T.L., Martín-Pintado, J., 1997, in preparation
- Irvine, W.M., Schloerb, F.P., Hjalmarsen, Å., Herbst, E., 1985, *The Chemical State of Dense Interstellar Clouds: An Overview*. In D.C. Black, M.S. Matthews (eds.), *Protostars & Planets II*. The University of Arizona Press, Tuscon, p. 579
- Ishizuki, S., Kawabe, R., Ishiguro, M., Okumura, S.K., Morita, K.-I., Chikada, Y., Kasuga, T., 1990, *Nature* 344, 224
- Ishizuki, S., Kawabe, R., Ishiguro, M., Okumura, S.K., Morita, K.-I., Chikada, Y., Kasuga, T., Wright, M.C.H., 1991, *High Resolution  $^{12}\text{CO}$  and  $^{13}\text{CO}$  Images of the Central Region of IC 342*. In F. Combes, F. Casoli (eds.), *Dynamics of Galaxies and their Molecular Cloud Distribution*, IAU Symp. 146, 272
- Kaifu, N., Kato, T., Iguchi, T., 1972, *Nature Physical Science* 238, 105
- Lindqvist, M., Sandqvist, A., Winnberg, A., Johansson, L.E.B., Nyman, L.-Å., 1995, *A&AS* 113, 257
- Lis, D.C., Carlstrom, J.E., 1994, *ApJ* 424, 189
- Mauersberger, R., Guélin, M., Martín-Pintado, J., Thum, C., Cernicharo, J., Hein, H., Navarro, S., 1989, *A&AS* 79, 217
- Mauersberger, R., Henkel, C., Wielebinski, R., Wiklind, T., Reuter, H.-P., 1996, *A&A* 305, 421
- McCall, M.L., 1989, *AJ* 97, 1341
- Mezger, P.G., Chini, R., Kreysa, E., Gemünd, H.-P., 1986, *A&A* 160, 324
- Oka, T., Hasegawa, T., Hayashi, M., Handa, T., Sakamoto, S., 1997, to appear in *ApJ*
- Paglionone, T.A.D., Tosaki, T., Jackson, J.M., 1995, *ApJ* 454, L117
- Pence, W.D., 1981, *ApJ* 247, 473
- Penzias, A.A., 1980, *Science* 208, 663
- Phillips, T.J., Huggins, P.J., Wannier, P.G., Scoville, N.Z., 1979, *ApJ* 231, 720
- Rieke, G., Lebofsky, M., Walker, C., 1988, *ApJ* 325, 679
- Rohlfs, K., Wilson, T.L., 1996, *Tools of Radio Astronomy*, 2nd ed., Springer, Berlin – Heidelberg
- Rougeer, G.W., Oort, J.H., 1960, *Proc. Nat. Acad. Sci.* 46, 1
- Sanders, D.B., Solomon, P.M., Scoville, N.Z., 1984, *ApJ* 276, 182
- Scoville, N.Z., 1972, *ApJ* 175, L127
- Shier, L.M., Rieke, M.J., Rieke, G.H., 1994, *ApJ* 433, L9
- Silk, J., Bloemen, H., 1987, *ApJ* 313, L47
- Sodroski, T.J., Bennett, C., Boggess, N., Dwek, E., Franz, B.A., Hauser, M.G., Kelsall, T., Moseley, S.H., Odegard, N., Silverberg, R.V., Weiland, J.L., 1994, *ApJ* 428, 638
- Solomon, P.M., Rivolo, A.R., Barrett, J.W., Yahil, A., 1987, *ApJ* 319, 730
- Stark, A.A., Bania, T.M., 1986, *ApJ* 306, L17
- Strong, A.W., Bloemen, J.B.G.M., Dame, T.M., Grenier, I.A., Hermsen, W., Lebrun, F., Nyman, L.-Å., Pollock, A.M.T., Thaddeus, P., 1988, *A&A* 207, 1
- Taylor, S.D., Hartquist, T.W., Williams, D.A., 1993, *MNRAS* 264, 929
- Turner, J.L., Hurt, R.L., 1992, *ApJ* 384, 72
- Wilson, T.L., Matteucci, F., 1992, *A&AR* 4, 1
- Wilson, T.L., Rood, R.T., 1994, *ARA&A* 32, 191
- Young, J.S., Scoville, N.Z., 1982, *ApJ* 258, 467

## Appendix

### A. Detailed Discussion of Figures

#### A.1. Spectral Line Shapes in Fig. 3

In Fig. 3, spectra of both  $^{12}\text{CO}$  and  $\text{C}^{18}\text{O}$  toward characteristic emission centers are shown: four examples of single positions toward the Galactic bulge and two averaged over several positions of Clump 2 (Bania 1977). In this section, we discuss the presented spectra in detail particularly emphasizing the applicability of the SCF to the molecular gas in the Galactic center region. Besides comparing the spectra of the two CO isotopomers in detail we make LTE estimates using the equations given in Section 14.8.1 of Rohlfs & Wilson (1996). For a detailed derivation in the case of  $\text{C}^{18}\text{O}$ , in particular taking into account that all data refer to the area of the telescope beam which is not infinitesimally small, see Dahmen (1995).

#### A.1.1. Sgr A Region

In plot (a) of Fig. 3, the  $^{12}\text{CO}(1-0)$  and the  $\text{C}^{18}\text{O}(1-0)$  spectra toward  $l = 0^\circ 0'$ ,  $b = 0^\circ 0'$ , near Sgr A, are shown. Even though averaged over the  $9'$ -telescope beam, there is considerable fine structure in the spectra and the line shapes in  $^{12}\text{CO}$  and  $\text{C}^{18}\text{O}$  are very different. The two minima (B) and (D) in  $^{12}\text{CO}$  do not have counterparts in  $\text{C}^{18}\text{O}$ . The minimum (D) coincides with the  $\text{C}^{18}\text{O}$  maximum (a), the most intense feature in  $\text{C}^{18}\text{O}$  at this position. Therefore, it is likely that the minima (B) and (D) in the  $^{12}\text{CO}$  emission are caused by self absorption. Because of the rather narrow line widths, this gas is likely to be local. Then, (A) and (C) show up as maxima just because self absorption effects are minimal.

The so-called Expanding Molecular Ring (EMR; see Scoville 1972; Kaifu et al. 1972) is only marginally visible in  $\text{C}^{18}\text{O}$ , but is rather intense in  $^{12}\text{CO}$ , especially at positive velocities.

At positive velocities, broad emission is present both in  $^{12}\text{CO}$  and  $\text{C}^{18}\text{O}$ . The  $^{12}\text{CO}$  maximum (E) coincides

roughly with maximum (b) of  $\text{C}^{18}\text{O}$ . However, the most intense  $^{12}\text{CO}$  maximum (F) is only present as an emission wing in  $\text{C}^{18}\text{O}$ . Because of the large velocity extent, it is certain that these features arise in the Galactic center, but the excitation of (E) and (F) must be different. If the SCF (Eq. 1) applies, the shapes of the  $^{12}\text{CO}$  and the  $\text{C}^{18}\text{O}$  lines should be the same. Because this is obviously not the case, one or more of the requirements of this factor are not fulfilled (see also Section 3.2). This alone is proof that the  $J = 1 \rightarrow 0$  lines of  $^{12}\text{CO}$  and  $\text{C}^{18}\text{O}$  *cannot* both trace the total  $\text{H}_2$  mass, as it is commonly assumed for disk clouds.

### A.1.2. Sgr B2 Region

In plot (b) of Fig. 3, we present the spectra of the  $^{12}\text{CO}(1-0)$  and the  $\text{C}^{18}\text{O}(1-0)$  transition toward the position ( $l = +0^\circ6$ ,  $b = 0^\circ0$ ) near Sgr B2. In  $^{12}\text{CO}$ , six maxima can be recognized. Four of these are associated with the main Galactic center emission and two with the EMR. In general, the  $\text{C}^{18}\text{O}$  emission shows the same line shape as the  $^{12}\text{CO}$  emission. The EMR peaks, which are the weakest features in  $^{12}\text{CO}$ , are below our detection limit for  $\text{C}^{18}\text{O}$ . Thus, for this position the SCF might be applicable. However, compared to  $^{12}\text{CO}$ , the peak components seem narrower and more pronounced over the extended background in  $\text{C}^{18}\text{O}$ .

To check if the SCF is applicable, we evaluate the conversion factors in detail for this position. The integrated intensities from  $-225.0$  to  $+225.0 \text{ km s}^{-1}$  are  $25.3 \text{ K km s}^{-1}$  for  $\text{C}^{18}\text{O}(1-0)$  and  $1560 \text{ K km s}^{-1}$  for  $^{12}\text{CO}(1-0)$ . From the SCF (Eq. 1, assuming  $^{12}\text{CO}/\text{H}_2 = 10^{-4}$ ) one finds the column density of  $^{12}\text{CO}$  as:

$$\bar{\mathcal{N}}_{^{12}\text{CO}}(\text{SCF}) = 3.59 \cdot 10^{19} \text{ cm}^{-2} \quad (\text{A1})$$

To derive the column density of  $\text{C}^{18}\text{O}$ , the excitation temperature and beam-filling factor  $f_{\text{beam}}$  of CO must be estimated. If the SCF can be applied, the  $^{12}\text{CO}(1-0)$  line must be optically thick. Assuming that the excitation of the CO(1-0) transitions is close to LTE and that the excitation temperature is the same for both isotopomers, the relations from Rohlfs & Wilson (1996)/Dahmen (1995) can be used.

To apply these to our data, we need the beam filling factor,  $f_{\text{beam}}$ , both for  $\text{C}^{18}\text{O}$  and  $^{12}\text{CO}$ . For  $\text{C}^{18}\text{O}$ ,  $f_{\text{beam}}$  can be estimated by comparing our data with higher angular resolution data. Lindqvist et al. (1995) presented  $\text{C}^{18}\text{O}(1-0)$  data of the Sgr A region obtained with the 15 m SEST telescope with a resolution of  $45''$ . Their integrated intensity toward the peak of the Sgr A complex is  $\sim 50 \text{ K km s}^{-1}$  (on a  $T_{\text{MB}}$ -scale). Compared to our value of  $17.3 \text{ K km s}^{-1}$ , we estimate  $f_{\text{beam}}$  for  $\text{C}^{18}\text{O}(1-0)$  to be:

$$f_{9'-\text{beam}}^{\text{C}^{18}\text{O}} \approx 0.3 \quad (\text{A2})$$

For the smoother and more widespread  $^{12}\text{CO}(1-0)$  emission (see Fig. 2 and the  $^{12}\text{CO}$  presentation in Paper I), we estimate a beam-filling factor of:

$$f_{9'-\text{beam}}^{^{12}\text{CO}} \approx 0.5 \quad (\text{A3})$$

Using the assumptions mentioned above, the excitation temperature  $T_{\text{ex}}$  is obtained from the  $^{12}\text{CO}(1-0)$  data. With  $T_{\text{MB}}$  of  $^{12}\text{CO}(1-0)$  ranging from 2 K to 13.5 K, this results in a  $T_{\text{ex}}$  from 7 K to 30 K, typically 20 K. For  $\text{C}^{18}\text{O}(1-0)$ , the emission is found to be optically thin, and  $T_{\text{MB}}$  is typically 0.2 K. Then, the beam-averaged column density is:

$$\bar{\mathcal{N}}_{\text{C}^{18}\text{O}}(T_{\text{ex}} = 20 \text{ K}) = 2.65 \cdot 10^{16} \text{ cm}^{-2} \quad (\text{A4})$$

These column densities result in a  $^{16}\text{O}/^{18}\text{O}$  isotope ratio of  $\sim 1350$ , 2.7 times what is found in the local ISM and in sharp contradiction to the value of 250 commonly adopted for the Galactic center (Wilson & Matteucci 1992; Wilson & Rood 1994).

To force agreement between the column densities of  $\text{C}^{18}\text{O}$  and  $^{12}\text{CO}$ , one could revise the SCF or raise  $T_{\text{ex}}$  to 120 K. This high a  $T_{\text{ex}}$  agrees with the  $T_{\text{kin}}$  found for 34 Galactic center cloud peaks (Hüttemeister et al. 1993) in  $\text{NH}_3$ . LVG radiative transfer calculations for the same cloud sample, applied to  $\text{C}^{18}\text{O}(1-0)$  and  $\text{C}^{18}\text{O}(2-1)$  lines (Hüttemeister 1993, chapt. 5) give similar temperatures. However, if  $T_{\text{ex}}$  is this high, the beam averaged  $^{12}\text{CO}$  emission *cannot* be optically thick, because then  $T_{\text{MB}}$  should be  $\sim 100 \text{ K}$  and more which is clearly not the case. Thus, the SCF *cannot* be applied to  $^{12}\text{CO}$ . On the other hand, if the  $^{12}\text{CO}$  emission *is* optically thick,  $T_{\text{ex}}$  can be *at most* 30 K. Then, the SCF for  $^{12}\text{CO}$  *does not* apply because the column density of  $^{12}\text{CO}$  is, even in the integration over the complete velocity range, too large by a factor of  $\sim 5$  compared to  $\text{C}^{18}\text{O}$ .

In conclusion, even toward a position where, at first glance, it seems that the SCF might be valid, it is shown that this is not the case. This conclusion is even stronger if one considers other positions.

### A.1.3. Sgr C Region

Near Sgr C (plot (c) of Fig. 3), the most prominent feature in  $^{12}\text{CO}(1-0)$  both in peak intensity and line width is the emission of the EMR. The main emission (B to C) is rather weak, and, in addition, there is a narrow peak (A) which is probably of local origin.

In  $\text{C}^{18}\text{O}$ , the features of the EMR are not visible. The main Galactic center component is very similar to what is seen in  $^{12}\text{CO}$  (b to c). The narrow peak (a) coincides almost exactly with the respective  $^{12}\text{CO}$  peak (A), but is more pronounced. The additional (though tentative), narrow peak (d) corresponds to the 3-kpc-arm (Rougeot & Oort 1960) emission and has no counterpart in  $^{12}\text{CO}$ ; this

is probably superposed on the more intense main component. Such behaviour is typical and is observed toward several positions.

These spectra confirm that the excitation conditions vary strongly with velocity. In addition, the discrepancy between the column density of  $^{12}\text{CO}$ , determined from the SCF, and the column density, determined for the optically thin  $\text{C}^{18}\text{O}$  emission, is even larger than toward Sgr B2.

#### A.1.4. Sgr D Region

Toward Sgr D, the  $l = 1^\circ 5$ -complex of Bally et al. (1988) (plot (d) of Fig. 3), the line profiles in  $^{12}\text{CO}(1-0)$  and  $\text{C}^{18}\text{O}(1-0)$  agree very well. The intense maxima (A/a) coincide, and the different velocity extent (B to C in  $^{12}\text{CO}$  and b to c in  $\text{C}^{18}\text{O}$ ) can be explained with the lower signal-to-noise ratio in the  $\text{C}^{18}\text{O}$  spectrum. This is also likely for the EMR peak only visible in  $^{12}\text{CO}$ . However, applying the same scheme as in Appendix A.1.2, it can again be shown that the SCF is not applicable for this region.

Therefore, we will investigate the possibility whether such good agreement in line shape can be explained by a *low* optical depth, even for  $^{12}\text{CO}(1-0)$  emission. We find for the intensities integrated over the velocity range from  $-225.0$  to  $+225.0 \text{ km s}^{-1}$   $10.3 \text{ K km s}^{-1}$  in case of  $\text{C}^{18}\text{O}(1-0)$  and  $1270 \text{ K km s}^{-1}$  in case of  $^{12}\text{CO}(1-0)$ . It is unlikely that the  $^{12}\text{CO}$  emission is truly optically thin. However, we can assume that the optical depth is of order unity, as is consistent with the nearly identical line shape. Then Eq. 8 holds, and the beam-averaged column density of  $^{12}\text{CO}$  is given by:

$$\bar{\mathcal{N}}_{12\text{CO}} = \frac{2.31 \cdot 10^{14} \text{ cm}^{-2}}{\text{K km s}^{-1}} \cdot \frac{\tau_0^{12\text{CO}(1-0)}}{1 - e^{-\tau_0^{12\text{CO}(1-0)}}} \cdot \frac{\int T_{\text{MB}}^{12\text{CO}(1-0)}(v) dv}{1 - \exp(-5.53 \text{ K}/T_{\text{ex}})} \quad (\text{A5})$$

Adopting the standard  $^{16}\text{O}/^{18}\text{O}$  ratio in the Galactic center, one can set this expression equal to 250 times the column density of the optically thin  $\text{C}^{18}\text{O}$  and solve for the optical depth:

$$\frac{\tau_0^{12\text{CO}(1-0)}}{1 - e^{-\tau_0^{12\text{CO}(1-0)}}} = \frac{2.43 [1 - \exp(-5.53 \text{ K}/T_{\text{ex}})]}{2.31 [1 - \exp(-5.27 \text{ K}/T_{\text{ex}})]} \cdot \frac{250 \int T_{\text{MB}}^{\text{C}^{18}\text{O}(1-0)}(v) dv}{\int T_{\text{MB}}^{12\text{CO}(1-0)}(v) dv} \quad (\text{A6})$$

Note that  $f_{\text{beam}}$  plays no role as long as the beam and cloud sizes are comparable. The dependence on  $T_{\text{ex}}$  is weak and the fraction containing it is equal to  $\sim 1.1$ . Therefore, the optical depth of the  $^{12}\text{CO}$  emission can be determined from the integrated intensities and one obtains:

$$\tau_0^{12\text{CO}(1-0)}(l = 1^\circ 2, b = 0^\circ 0) \approx 1.9 \quad (\text{A7})$$

Thus, surprisingly, moderate optical depths are obtained from an analysis of the data, even for one of the most intense  $^{12}\text{CO}$  peaks in the Galactic center region.

#### A.1.5. Northern Clump 2 Region

From Figs. 5 and 15 in Paper I, we noted that the velocity structure of the northern and the southern region of Clump 2 might be completely different. A detailed analysis of the spectra shows that this is indeed the case. Therefore, we averaged Clump 2 spectra separately for the northern and the southern part. The positions included in the averages were chosen for both parts from the presence of at least some  $\text{C}^{18}\text{O}$  emission and of similar velocity structure, as suggested by Fig. 5 in Paper I.

In plot (e) of Fig. 3, we show the average of 14 positions toward the northern region of Clump 2. In  $^{12}\text{CO}$ , this northern Clump 2 region shows a broad plateau of emission (B to C) from about  $-30$  to  $+180 \text{ km s}^{-1}$ . It has a nearly constant intensity of some  $2.5 \text{ K}$ , except for the strong peak (A) at  $\sim +20 \text{ km s}^{-1}$  with an intensity of about  $4.3 \text{ K}$ . Two weak side peaks (D and E) at  $\sim -70$  and  $\sim -45 \text{ km s}^{-1}$  can be recognized. Peak (E) probably belongs to the 3-kpc-arm because its velocity matches the expected velocity of this feature at this Galactic longitude (Bania 1977, 1980, 1986).

In  $\text{C}^{18}\text{O}$ , the emission is very weak, indicating (as discussed) moderate to low optical depth in  $^{12}\text{CO}$  emission. Thus, the total molecular mass of Clump 2 will be significantly less than suggested by the SCF. The only feature clearly visible in  $\text{C}^{18}\text{O}$  is the peak (a) at  $\sim +20 \text{ km s}^{-1}$  with wings (b to c) from about  $+5$  to  $+60 \text{ km s}^{-1}$ , similar to peak (A) and its wings visible in  $^{12}\text{CO}$ . Other features visible in  $^{12}\text{CO}$  are obviously too weak to show up in  $\text{C}^{18}\text{O}$ .

#### A.1.6. Southern Clump 2 Region

In plot (f) of Fig. 3, we show the average of 8 positions toward the southern region of Clump 2.

In the  $^{12}\text{CO}$  spectrum of this region of Clump 2, 5 maxima can be clearly distinguished. The two more intense ones (C and E) are at about  $+5$  and  $+95 \text{ km s}^{-1}$ ; the weaker features are at about  $-40$ ,  $-25$ , and  $+45 \text{ km s}^{-1}$ . The EMR tends to be found at more negative latitudes and more positive velocities toward more positive longitudes. In this plot, it appears with a peak at about  $+225 \text{ km s}^{-1}$ . Note the weak emission which connects the EMR tail with the main emission components and the weak extended wing toward velocities as negative as  $-110 \text{ km s}^{-1}$ .

In  $\text{C}^{18}\text{O}$ , peak (b) at about  $+105 \text{ km s}^{-1}$  is the only clearly visible feature. It roughly coincides with the  $^{12}\text{CO}$  peak (E) although the maximum is at higher velocities. Another peak, (a), may be present at about  $+20 \text{ km s}^{-1}$ . However, around about  $-5 \text{ km s}^{-1}$ , the spectrum seems to show some artifacts. In addition, there is no counterpart

peak visible in  $^{12}\text{CO}$ . Thus, this emission may be spurious. However, this peak appears at the same velocity as peak (a) in the northern part of Clump 2. Because we have already found lacks of agreement between  $^{12}\text{CO}$  and  $\text{C}^{18}\text{O}$ , this feature could indicate a component present over the entire Clump 2.

### A.2. The Features in Fig. 5

In Fig. 5, the ratio of the intensity of  $^{12}\text{CO}(1-0)$  to  $\text{C}^{18}\text{O}(1-0)$  emission in the Galactic center region, integrated over velocity intervals of  $50 \text{ km s}^{-1}$ , is displayed. Here we give a detailed description of the plots.

At  $-150 \text{ km s}^{-1}$  and at  $-100 \text{ km s}^{-1}$ , the Sgr C region is most prominent. It shows high ratios reaching  $> 75$ , peaking with a ratio of  $\sim 90$  at  $(l = -0^\circ 47, b = +0^\circ 13)$  and  $(l = -0^\circ 6, b = 0^\circ 0)$ , respectively. Most of the data points are lower limits. However, the ratio of the maximum of the Sgr C region at  $-100 \text{ km s}^{-1}$  is an actual value, not merely a limit.

At  $-50 \text{ km s}^{-1}$  (the 3-kpc-arm) and  $0 \text{ km s}^{-1}$  (the widespread component of the Galactic center, but also local gas), no very high ratios are found. However, the ratios show much structure, and typically range from 30 to 80 in the areas where  $\text{C}^{18}\text{O}$  is above the detection limit (refer to Fig. 5 in Paper I). Note, that at  $-50 \text{ km s}^{-1}$ , the Sgr A region and the region at  $(l = +0^\circ 9, b = 0^\circ 0)$  appear as valley-like minima with ratios  $< 40$ . These are not lower limits and are surrounded by rims of higher ratios. At  $0 \text{ km s}^{-1}$ , the same effect can be seen again in the Sgr A region as well as in the Sgr B2 and in the region at  $(l = +1^\circ 05, b = -0^\circ 15)$ .

In the velocity ranges centered at  $+50 \text{ km s}^{-1}$  and at  $+100 \text{ km s}^{-1}$ , the ratio reaches values of 90 to 120 in large areas, and in a few positions these are higher still, reaching values  $> 200$ . The most prominent areas are the Sgr D region (the  $l = 1^\circ 5$ -complex of Bally et al. 1988) and Clump 2. In the Sgr D region, ratios of 90 to 120 are reached at  $+50 \text{ km s}^{-1}$  in the area from  $l = +1^\circ 1$  to  $+1^\circ 8$  and from  $b = -0^\circ 35$  to  $+0^\circ 2$  peaking at  $(l = +1^\circ 4, b = -0^\circ 15)$  with a ratio of  $> 200$  and at  $+100 \text{ km s}^{-1}$  in the area from  $l = +0^\circ 9$  to  $+1^\circ 6$  and from  $b = -0^\circ 3$  to  $+0^\circ 45$  peaking at  $(l = +1^\circ 5, b = +0^\circ 3)$  also with a ratio of  $> 200$ . In Clump 2 at  $+50 \text{ km s}^{-1}$ , the ratio reaches such high values in the area from  $l = +3^\circ 0$  to  $+3^\circ 35$  and from  $b = +0^\circ 3$  to  $+0^\circ 65$  peaking at  $(l = +3^\circ 3, b = +0^\circ 5)$  with a ratio of nearly 170. At  $+100 \text{ km s}^{-1}$ , such high ratios are achieved in the area from  $l = +2^\circ 9$  to  $+3^\circ 35$  and from  $b = -0^\circ 05$  to  $+0^\circ 65$  peaking at  $(l = +3^\circ 15, b = +0^\circ 15)$  with a ratio of  $\sim 160$ . The absolutely highest ratio over all velocities is the maximum of the Sgr D region at  $+100 \text{ km s}^{-1}$ . In addition, there are 2 definite valley-like minima, where the determined ratios are not lower limits. These minima are the Sgr B2 region at  $+50 \text{ km s}^{-1}$  (ratio  $\lesssim 40$ ) and the region around  $(l = +1^\circ 05, b = 0^\circ 0)$  at  $+100 \text{ km s}^{-1}$  (ratio  $\sim 70$ ). Both regions coincide with

maxima in the  $\text{C}^{18}\text{O}$  emission and are surrounded by areas with higher ratios.

At  $+150 \text{ km s}^{-1}$  and even more at  $+200 \text{ km s}^{-1}$ , almost all ratios are lower limits. However, at  $+150 \text{ km s}^{-1}$  there are two regions where even the lower limit of the ratio exceeds 90, namely toward  $(l = -0^\circ 75, b = +0^\circ 05)$  near the Sgr C region and toward  $(l = +0^\circ 45, b = +0^\circ 3)$ . Toward three further regions, the ratio reaches values of about 75, i.e. toward  $(l = +0^\circ 15, b = +0^\circ 15)$  near the Sgr A region toward  $(l = +1^\circ 35, b = +0^\circ 4)$  near the Sgr D region and toward  $(l = +1^\circ 2, b = -0^\circ 15)$ . Most prominent at  $+150 \text{ km s}^{-1}$  is Clump 2 where ratios of 90 to 120 are found in the area  $l = +2^\circ 95$  to  $+3^\circ 35$  and from  $b = 0^\circ 0$  to  $+0^\circ 55$  peaking at  $(l = +3^\circ 15, b = +0^\circ 15)$  with a ratio of about 135 where the ratio is a real value and not a lower limit. Valley-like minima surrounded by areas with higher ratios are present at  $(l = +1^\circ 0, b = +0^\circ 1, \text{ratio} \sim 20)$  close to the minimum at  $+100 \text{ km s}^{-1}$  and at  $(l = +1^\circ 5, b = 0^\circ 0)$  where even no  $^{12}\text{CO}$  emission is found.